

AD-750 553

A STUDY OF ELECTRON COLLISION FREQUENCY  
IN AIR MIXTURES AND TURBULENT BOUNDARY

Dennis W. Lankford

Air Force Weapons Laboratory  
Kirtland Air Force Base, New Mexico

October 1972

DISTRIBUTED BY:

**NTIS**

National Technical Information Service  
U. S. DEPARTMENT OF COMMERCE  
5285 Port Royal Road, Springfield Va. 22151

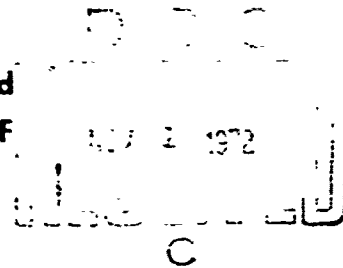
AD 750553

AFWL-TR-72-71

AFWL-TR-  
72-71

**A STUDY OF ELECTRON COLLISION  
FREQUENCY IN AIR MIXTURES  
AND TURBULENT BOUNDARY  
LAYERS WITH ABLATION**

Dennis W. Lankford  
Sgt USAF



TECHNICAL REPORT NO. AFWL-TR-72-71

October 1972

**AIR FORCE WEAPONS LABORATORY**  
Air Force Systems Command  
Kirtland Air Force Base  
New Mexico

Reproduced by  
NATIONAL TECHNICAL  
INFORMATION SERVICE  
U.S. Department of Commerce  
Springfield, A 22151

Approved for public release; distribution unlimited.



67

AFWL-TR-72-71

AIR FORCE WEAPONS LABORATORY  
Air Force Systems Command  
Kirtland Air Force Base  
New Mexico 87117

ACCESSION NO.	
NTIS	Write Section <input checked="" type="checkbox"/>
DDC	Ref. Section <input type="checkbox"/>
EXTRACTED	<input type="checkbox"/>
JUSTIFICATION	
BY	
DISTRIBUTION/AVAILABILITY CODES	
Dist.	Avail. & Use Special
A	

When US Government drawings, specifications, or other data are used for any purpose other than a definitely related Government procurement operation, the Government thereby incurs no responsibility nor any obligation whatsoever, and the fact that the Government may have formulated, furnished, or in any way supplied the said drawings, specifications, or other data, is not to be regarded by implication or otherwise, as in any manner licensing the holder or any other person or corporation, or conveying any rights or permission to manufacture, use, or sell any patented invention that may in any way be related thereto.

DO NOT RETURN THIS COPY. RETAIN OR DESTROY.

UNCLASSIFIED

Security Classification

DOCUMENT CONTROL DATA - R & D

Security classification of title, body of abstract and indexing information must be entered when the overall report is classified.

1 ORIGINATING ACTIVITY (Corporate author) Air Force Weapons Laboratory (DYT) Kirtland Air Force Base, New Mexico 87117		2a. REPORT SECURITY CLASSIFICATION Unclassified	
3 REPORT TITLE A STUDY OF ELECTRON COLLISION FREQUENCY IN AIR MIXTURES AND TURBULENT BOUNDARY LAYERS WITH ABLATION			
4 DESCRIPTIVE NOTES (Type of report and inclusive dates) May 1970 through March 1971			
5 AUTHOR(S) (First name, middle initial, last name) Dennis W. Lankford, Sgt, USAF			
6 REPORT DATE October 1972	7a TOTAL NO OF PAGES 64	7b NO OF REFS 24	
8a CONTRACT OR GRANT NO 9 PROJECT NO 5791		10. ORIGINATOR'S REPORT NUMBER(S) AFWL-TR-72-71	
8c		11 OTHER REPORT NO(S) (Any other numbers that may be assigned this report)	
11 DISTRIBUTION STATEMENT Approved for public release; distribution unlimited.			
12 SUPPLEMENTARY NOTES		12 SPONSORING MILITARY ACTIVITY AFWL (DYT) Kirtland AFB, NM 87117	
13 ABSTRACT (Distribution Limitation Statement A) The electron collision frequency is a critical parameter in determining the attenuation of electromagnetic signals transmitted through the plasma sheath surrounding advanced reentry vehicles. This study improves current methods of obtaining this parameter for multicomponent gas mixtures. A multicomponent collision frequency model is defined with temperature and species-dependent electron collision cross sections. A parametric study of collision frequency in a gaseous mixture of phenolic carbon and air is performed using this model, and the results are compared to calculations made using a constant cross-section, clean air model. A study of collision frequency and signal attenuation in turbulent boundary layers is performed using the multicomponent and constant cross-section models. This study shows that the multicomponent model can predict collision frequencies in an ablation air mixture that are significantly different from those predicted by constant cross-section models. These differences can result from large cross-section ablation molecules or from the temperature dependence of the multicomponent cross sections. The effect these frequency differences have upon the signal attenuation are dependent on the electron density profiles. The attenuation predicted by the two models may or may not differ significantly.			

1a

14 KEY WORDS	LINK A		LINK B		LINK C	
	ROLE	WT	ROLE	WT	ROLE	WT
Boundary layer Collision frequency Plasma						
<i>Ib</i>						

AFWL-TR-72-71

A STUDY OF ELECTRON COLLISION FREQUENCY IN AIR MIXTURES  
AND TURBULENT BOUNDARY LAYERS WITH ABLATION

Dennis W. Lankford  
Sgt USAF

TECHNICAL REPORT NO. AFWL-TR-72-71

Approved for public release; distribution unlimited.

IC

FOREWORD

This report was prepared under Project 579i, Program Element 62301F.

Inclusive dates of research were May 1970 through March 1971. The report was submitted 28 July 1972 by the Air Force Weapons Laboratory Project Officer, Sgt Dennis W. Lankford (DYT)

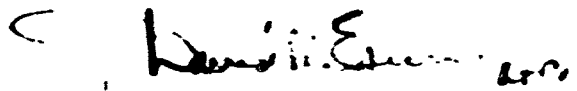
This report has been reviewed and is approved.



DENNIS W. LANKFORD  
Sgt, USAF  
Project Officer



JAY R. ROLAND  
Major, USAF  
Chief, Theoretical Physics Branch



DURWARD D. YOUNG, JR.  
Lt Colonel, USAF  
Chief, Technology Division

## ABSTRACT

(Distribution Limitation Statement A)

The electron collision frequency is a critical parameter in determining the attenuation of electromagnetic signals transmitted through the plasma sheath surrounding advanced reentry vehicles. This study improves current methods of obtaining this parameter for multicomponent gas mixtures. A multicomponent collision frequency model is defined with temperature and species-dependent electron collision cross sections. A parametric study of collision frequency in a gaseous mixture of phenolic carbon and air is performed using this model, and the results are compared to calculations made using a constant cross-section, clean air model. A study of collision frequency and signal attenuation in turbulent boundary layers is performed using the multicomponent and constant cross-section models. This study shows that the multicomponent model can predict collision frequencies in an ablation air mixture that are significantly different from those predicted by constant cross-section models. These differences can result from large cross-section ablation molecules or from the temperature dependence of the multicomponent cross sections. The effect these frequency differences have upon the signal attenuation are dependent on the electron density profiles. The attenuation predicted by the two models may or may not differ significantly.

## CONTENTS

<u>Section</u>		<u>Page</u>
I	INTRODUCTION	1
II	METHODOLOGY	3
	Signal Attenuation Calculation	3
	Collision Frequency Calculation	4
	Electron-Particle Collision Cross Section	5
	Literature Survey	6
III	PARAMETRIC STUDY	9
IV	STUDY OF TURBULENT BOUNDARY LAYERS	23
	High-Velocity Reentry Trajectory; Cases 1 to 6	23
	Reentry Case Analyzed by BLIMP Code; Case 7	38
	Rocket Sled; Case 8	44
V	CONCLUSIONS AND RECOMMENDATIONS	50
	References	53

## ILLUSTRATIONS

<u>Figure</u>		<u>Page</u>
1	Collision Cross Sections for Molecular Species Present in a Mixture of Phenolic Carbon and Air	8
2	Parametric Study--Collision Frequency at 0.1 Atmospheres Pressure with Mass Fraction of Ablator Varying from 0 to 50 Percent	11
3	Parametric Study--Collision Frequency at 0.5 Atmospheres Pressure with Mass Fraction of Ablator Varying from 0 to 50 Percent	12
4	Parametric Study--Collision Frequency at 1.0 Atmospheres Pressure with Mass Fraction of Ablator Varying from 0 to 50 Percent	13
5	Parametric Study--Collision Frequency at 3.0 Atmospheres Pressure with Mass Fraction of Ablator Varying from 0 to 50 Percent	14
6	Parametric Study--Collision Frequency at 5.0 Atmospheres Pressure with Mass Fraction of Ablator Varying from 0 to 50 Percent	15
7	Parametric Study--Collision Frequency at Varying Ablator Mass Fraction with Temperature and Pressure Held Constant	16
8	Parametric Study--Mixture Composition at Varying Ablator Mass Fraction at 1.0 Atmosphere Pressure and 3135°R Temperature	17
9	Parametric Study--Mixture Composition at Varying Ablator Mass Fraction at 1.0 Atmosphere Pressure and 8360°R Temperature	18
10	Parametric Study--Mixture Composition at Varying Ablator Mass Fraction at 5.0 Atmospheres Pressure at 3135°R Temperature	19
11	Parametric Study--Mixture Composition at Varying Ablator Mass Fraction at 5.0 Atmospheres Pressure at 8360°R Temperature	20
12	Parametric Study--HCN Concentration in a Mixture with an Ablator Mass Fraction of 50 Percent at Pressures of 1.0 and 5.0 Atmospheres	21

## ILLUSTRATIONS (cont'd)

<u>Figure</u>		<u>Page</u>
13	Reentry Trajectory Case 1--Boundary Layer Collision Frequency Profile	25
14	Reentry Trajectory Case 2--Boundary Layer Collision Frequency Profile	26
15	Reentry Trajectory Case 3--Boundary Layer Collision Frequency Profile	27
16	Reentry Trajectory Case 4--Boundary Layer Collision Frequency Profile	28
17	Reentry Trajectory Case 5--Boundary Layer Collision Frequency Profile	29
18	Reentry Trajectory Case 6--Boundary Layer Collision Frequency Profile	30
19	Reentry Trajectory Study--Boundary Layer Temperature Profile	31
20	Reentry Trajectory Study--Boundary Layer Mass Fraction Profile	32
21	Reentry Trajectory Case 3--Boundary Layer Species Concentration Profiles	33
22	Reentry Trajectory Study--Boundary Layer Electron Concentration Profiles	34
23	Reentry Trajectory Study--Boundary Layer Signal Attenuation	35
24	Reentry Trajectory Study--Boundary Layer Signal Attenuation	36
25	Reentry Trajectory Case 3--Boundary Layer Electron Concentration and Collision Frequency Profiles	39
26	Nonsimilar Reentry Analysis--Boundary Layer Collision Frequency Profile	40
27	Nonsimilar Reentry Analysis--Boundary Layer Species Concentration Profiles	41
28	Nonsimilar Reentry Analysis--Boundary Layer Temperature Profile	42

## ILLUSTRATIONS (cont'd)

<u>Figure</u>		<u>Page</u>
29	Nonsimilar Reentry Analysis--Boundary Layer Electron Concentration Profile	43
30	Rocket Sled Analysis--Boundary Layer Collision Frequency Profile	46
31	Rocket Sled Analysis--Boundary Layer Temperature Profile	47
32	Rocket Sled Analysis--Boundary Layer Species Concentration Profiles	48
33	Rocket Sled Analysis--Boundary Layer Electron Concentration Profile	49

## SYMBOLS AND NOTATIONS

$C$	Speed of light (meters/second)
$E_I$	Input electric field (volts/meter)
$E_t$	Transmitted electric field (volts/meter)
$H_I$	Input magnetic field (amp/meters <sup>2</sup> )
$H_t$	Transmitted magnetic field (amp/meters <sup>2</sup> )
$K$	Boltzmann's constant ( $1.380 \times 10^{-16}$ erg/°K)
$k_0$	Propagation constant of free space (rad/meter) = $\omega/c$
$K_p$	Complex dielectric constant
$M$	Transmission matrix
$N_e$	Electron particle density (number of electrons/centimeter <sup>3</sup> )
$P$	Pressure (atmospheres)
$Q_c$	Collision cross section for elastic scattering (centimeters <sup>2</sup> )
$Q_{ej}$	Collision cross section for interaction between electron and molecular specie $j$ (centimeters <sup>2</sup> )
$Q_m$	Collision cross section for momentum transfer (centimeters <sup>2</sup> )
$T$	Temperature (degrees Kelvin)
$T_e$	Electron temperature (degrees Kelvin)
$\nu_c$	Electron collision frequency (seconds <sup>-1</sup> )
$d$	Slab thickness (meters)
$j$	Species identifier
$m_e$	Mass of 1 electron
$n_j$	Particle density of specie (number/centimeter <sup>3</sup> )
$ns$	Number of species
$p(\theta)$	Probability a particle will be scattered at an angle. $\theta$
$I(\theta)$	$p(\theta) \cdot Q_c$ by definition (centimeters <sup>2</sup> )

## SYMBOLS AND NOTATIONS

$z_p$	Characteristic impedance of plasma slab
$\gamma_p$	Propagation constant (radians/meter)
$\mu_0$	Permeability of free space
$\phi$	Azimuthal angle (radians)
$\theta$	Elevation angle (radians)
$\xi_0$	Angle of incidence (degrees)

## SECTION I

### INTRODUCTION

Hypersonic reentry vehicles encounter severe aerodynamic heating rates that necessitate ablative heatshield thermal protection to ensure vehicle survival. Unfortunately, the addition of heatshield material to the flow field surrounding a reentry vehicle may create a plasma that can seriously attenuate signals transmitted to or from the vehicle. This signal attenuation at radio frequencies can be principally attributed to reflection and absorption of the signal by free electrons in the flow field.

Heatshield materials are contaminated by small amounts of easily ionized chemical species, usually predominately sodium, that enter the flow field through ablation. Typically at altitudes below 100,000 feet, these ablation contaminates and the free electrons they produce are confined to the chemically reacting turbulent boundary layer that enshrouds the hypersonic vehicle. The plasma sheaths are typically collision-dominated since the charge particle densities are usually several orders of magnitude smaller than the neutral particle densities.

At a given signal frequency, the attenuation of a plasma sheath is characterized by electron density and electron collision-frequency profiles. Sophisticated computer codes can be used to determine chemical species and electron concentrations in chemically reacting turbulent boundary layers. Present methods for calculating electron collision frequencies in the plasma sheath formed on advanced hypersonic reentry vehicles are based on collision cross sections for high-temperature air (refs. 1 and 2). Since the ionized flow about these vehicles contains, in addition to air species, a number of ablation species with widely varying, temperature-dependent collision cross sections, the present electron collision frequency model may be inadequate for making accurate predictions of the plasma sheath electromagnetic signal attenuations.

This study defines an improved collision frequency model. The improved and present collision frequency models are compared in an investigation of the effect of ablation products in an air mixture on electron-neutral particle collision frequency. The two models are compared for a closed system parametric study and typical reentry vehicle boundary layers. Signal attenuation is calculated using the two models for a typical reentry vehicle.

The present collision frequency model employed in the Air Force Weapons Laboratory (AFWL) nonsimilar turbulent boundary layer code, BLIMP (ref. 3), and the AFWL similar turbulent boundary layer code, REBOUND (ref. 1), defines the electron-neutral collision cross section as a constant value representative of high-temperature clean air. Collision frequency is calculated with this one value of collision cross section, whereas the improved model defines the collision cross section as a function of temperature and the chemical species. Collision frequency is determined as the total of the collision frequencies for each specie. The improved model is thus physically more realistic than the present model.

SECTION II  
METHODOLOGY

1. SIGNAL ATTENUATION CALCULATION

To a first approximation, the attenuation of an electromagnetic signal on transmission through a plasma sheath can be calculated using a plane wave analysis (ref. 4). Plasma property variations are represented by dividing a plasma sheath into many slabs such that the properties of each slab can be assumed homogeneous. Each homogeneous slab is represented by its complex dielectric constant

$$K_p = 1 - \frac{\left(\frac{\omega_p}{\omega_s}\right)^2}{1 + \left(\frac{\nu_c}{\omega_s}\right)^2} - \frac{j\nu_c}{\omega_s} \cdot \frac{\left(\frac{\omega_p}{\omega_s}\right)^2}{1 + \left(\frac{\nu_c}{\omega_s}\right)^2} \quad (1)$$

where  $\omega_p = 56,000 \sqrt{N_e}$ . Thus, transmission through a slab is characterized by electron density ( $N_e$ ), collision frequency ( $\nu_c$ ), and the signal frequency ( $\omega_s$ ). The propagation constant for each slab is given by

$$\gamma_p = j k_0 \sqrt{K_p} \cos \theta_0 = j k_0 n_p \cos \theta_0 \quad (2)$$

For transverse waves the transmitted electric and magnetic fields are related to the input electric and magnetic fields of a single slab by the matrix equation

$$\begin{bmatrix} E_I \\ H_I \end{bmatrix} = \begin{bmatrix} \cosh \gamma_p d & -j Z_p \sinh \gamma_p d \\ \frac{j \sinh \gamma_p d}{Z_p} & \cosh \gamma_p d \end{bmatrix} \begin{bmatrix} E_T \\ H_T \end{bmatrix} \quad (3)$$

or

$$\begin{bmatrix} E_I \\ H_I \end{bmatrix} = M \begin{bmatrix} E_T \\ H_T \end{bmatrix} \quad (4)$$

where  $Z_p$  is the characteristic impedance of the slab given by

$$Z_p = \frac{\omega_s \mu_0}{\gamma_p} \quad (5)$$

The input and output fields for  $n$  homogeneous slabs are related, to a close approximation, by the product of the  $n$  transmission matrices for the slabs (ref. 4)

$$\begin{bmatrix} E_I \\ H_I \end{bmatrix} = \left( \prod_{i=1}^n M_i \right) \begin{bmatrix} E_T \\ H_T \end{bmatrix} \quad (6)$$

The total signal attenuation for a plasma sheath divided into  $n$  slabs can be determined from the above equation. Multiplying the logarithm of the ratio of the input power to the output power by ten gives the total attenuation in units of decibels.

## 2. COLLISION FREQUENCY CALCULATION

The collision frequency in a multicomponent ionized gas for electron-molecule, electron-atom, and/or electron-ion interactions is calculated (ref. 5) by

$$\nu_c = \sqrt{\frac{8kT_e}{\pi m_e}} \sum_{j=1}^{ns} n_j Q_{ej} \quad (7)$$

This equation is obtained assuming

- a. Maxwellian electron velocity distribution
- b. Particles (molecules, atoms, ions) are smooth, rigid, elastic spheres not surrounded by force fields

- c. Particles and electrons interact only at collision.
- d. Mixture of gases is at a uniform steady state.
- e. The mass and diameter of an electron are negligible compared to that of any molecule, atom, or ion.

Equation 6 indicates that collision frequency is dependent on electron velocity (i.e., temperature), and the summation of the product of each species population multiplied by its collision cross section. " $Q_{ej}$ " is the collision cross section for momentum transfer between an electron and specie  $j$ . It is dependent on electron temperature and the particular specie identity.

Ablation material and air may react to form a gaseous mixture consisting of a great number of chemical species. Inclusion of each species in equation 7 may not be possible because of a lack of collision cross-section data or excessive numbers of species. The product  $n_j Q_{ej}$  in equation 7 may be used to estimate the relative contribution of an individual specie to the total collision frequency. A number of species may be neglected in the collision frequency calculation, if the term  $\sum n_j Q_{ej}$  for the neglected species is small compared to  $\sum n_j Q_{ej}$  for the remaining species.

The equation presently used for calculating collision frequency in an ablation contaminated boundary layer is (ref. 1)

$$\nu = \frac{5.814 \times 10^{12} p}{T^{1/2}} \quad (8)$$

All the assumptions made for equation 7 apply to equation 8. Equation 8 can be derived from equation 7 with the additional assumption that the mixture is a single component ideal gas with a constant collision cross section which is representative of high-temperature air. A molecular diameter of  $3.65 \times 10^{-8}$  cm ( $10.4 \times 10^{-16}$  cm<sup>2</sup> cross section) and a molecular weight of 28.962 are used for this model.

### 3. ELECTRON-PARTICLE COLLISION CROSS SECTION

The probability that an elastic interaction will occur between an electron and a particle (atom, ion, or molecule) is defined (ref. 5) as the total elastic scattering collision cross section,  $Q_c$ . The probability that an electron will be scattered into a differential solid angle,  $d\Omega = \sin\theta d\theta d\phi$ , in an elastic

collision is  $p(\theta) \sin\theta d\theta d\phi$ . Defining  $I(\theta) \equiv p(\theta)Q_c$ , gives the differential scattering cross section,  $I(\theta) \sin\theta d\theta d\phi$ , and the total cross section for scattering.

$$Q_c = \int_0^\pi \int_0^{2\pi} I(\theta) \sin\theta d\theta d\phi \quad (9)$$

The energy lost in a momentum transfer collision by an electron scattered through an angle  $\theta$  is  $2(1-\cos\theta)m_e/m_j$ . Accordingly the collision cross section for momentum transfer is defined as

$$Q_m = \int_0^\pi \int_0^{2\pi} I(\theta) (1-\cos\theta) \sin\theta d\theta d\phi \quad (10)$$

If  $I(\theta)$  is independent of  $\theta$ , then the right hand sides of equations 9 and 10 can be integrated to show that  $Q_c = Q_m$ . This equality is approximately true for slow electrons (ref. 7). The electron velocities encountered by a typical reentry vehicle are sufficiently slow to assume  $Q_c = Q_m$  because thermal electron energies of less than 1 electron volt correspond to a typical reentry vehicle temperature range of 1000°R to 10,000°R. With this justification elastic scattering collision cross-section data were substituted for momentum transfer cross-section data when the latter were unavailable.

#### 4. LITERATURE SURVEY

A literature survey was performed to collect cross-section data for chemical species which might be found in an ablation mixture of heatshield material and air. Since phenolic carbon and phenolic silica are typical heatshield materials, documents containing cross-section data for molecules containing any combination of the elements C, H, N, O, A, and Si were collected (refs. 8 to 24). These cross-section data are also applicable to the AFWL rocket sled plasma experiment. The nose cone heatshield on the rocket sled is avcoat 8024 (epoxy urethane, C<sub>567</sub> H<sub>950</sub> O<sub>113</sub> N<sub>35</sub>) seeded with 20 percent by weight cesium nitrate. Collision data for the heatshield contaminants, sodium and cesium, were also collected.

Several sources of air collision data were located, but cross-section data for molecules containing silica, hydrogen, and/or carbon was limited. Shkarofsky,

Backynski, and Johnston (ref. 8) have collected and evaluated data from several sources for each of the air molecules N, NO, N<sub>2</sub>, O, O<sub>2</sub>, and A. This report guided the selection of air collision cross-section data used in the present study. Cross-section data for the following molecules containing hydrogen or carbon were collected: H, H<sub>2</sub>, H<sub>2</sub>O, HCN, C, CO, CO<sub>2</sub>, C<sub>2</sub>H<sub>4</sub>, C<sub>2</sub>H<sub>2</sub> (refs. 6, 9, 18, 19, 20, 23). Cesium and sodium cross-section data were available in reference 6 and 9. Only elemental silica cross-section data were found. The Bibliography of Low-Energy Electron Collision Cross-Section Data (refs. 10 and 11), a continuously updated guide to material on electron collisions, contained the only references found for the silica atom. Because data for molecules containing silica were not found, phenolic silica was not investigated in this study. The collected collision data are presented in figure 1.

Two sources were found that contain a considerable amount of collision data. Massey and Burhop (ref. 9) have compiled perhaps the most extensive set of collision cross-section data in their text, Electronic and Sonic Impact Phenomena. Brown (ref. 6) used a computer information retrieval system to compile cross-section data in Basic Data of Plasma Physics, 1966.

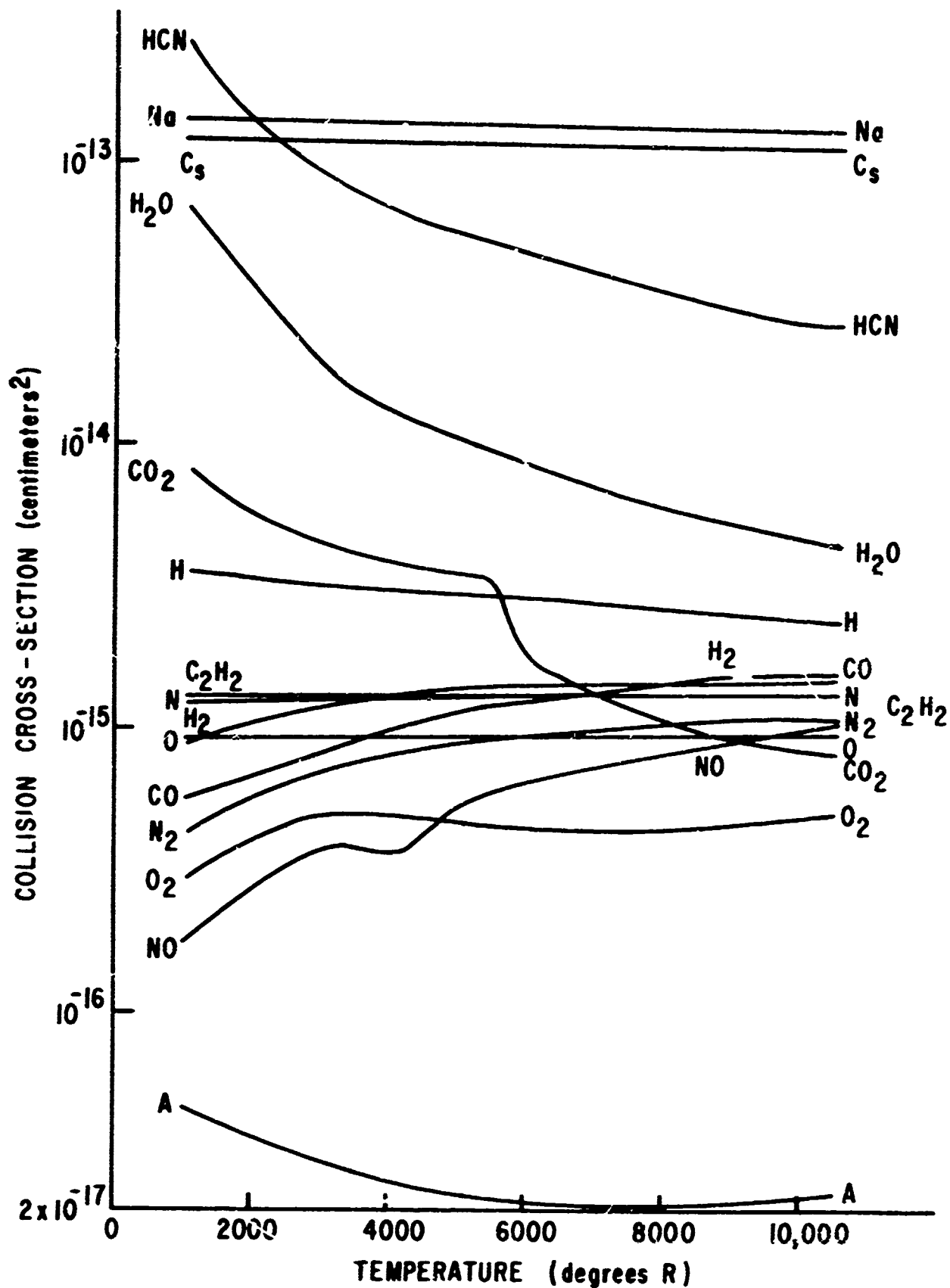


Figure 1. Collision Cross Sections for Molecular Species Present in a Mixture of Phenolic Carbon and Air

### SECTION III PARAMETRIC STUDY

A closed system parametric study was performed for a uniform gaseous mixture of phenolic carbon ( $C_7H_6O$ ) and air in chemical equilibrium. Temperature, pressure, and mass fraction of ablation material in the mixture were selected as the parameters of interest for this study. Parameter ranges were chosen to give system states typical of reentry boundary layers. System pressure was held constant at values of 0.1, 0.5, 1.0, 3.0, and 5.0 atmospheres, while collision frequency calculations were made varying temperature and the mass fraction of ablator. The temperature was varied from 1045°R to 10,450°R (corresponding to electron energies of 0.05 eV to 0.50 eV) and the mass fraction of ablator was varied from 0 to 50 percent.

The selection of chemical species to model the mixture was based on availability of cross-section data and particle concentrations in typical reentry boundary layers predicted by computer using a 60 species chemistry model. With reference to the discussion in section 2.2, the terms  $n_j Q_{ej}$  were used to determine which chemical species could be neglected in the collision frequency calculations. Since cross-section data were not available for every species, an upper limit for collision cross section was assumed equal to the largest cross section found in the literature. The largest cross section found was  $6020 \times 10^{-16} \text{ cm}^2$  for the large dipolar molecule  $CH_3NO_2$  at 295°K (ref. 18). This upper limit is approximately three orders of magnitude larger than the cross section of the density dominant  $N_2$  molecule in a turbulent boundary layer. To limit the magnitude of the term  $\sum n_j Q_{ej}$  for the rejected species to a small fraction of the term  $\sum n_j Q_{ej}$  for the considered species, only species having particle densities five or more orders of magnitude smaller than the density of  $N_2$  were eliminated from the collision frequency calculations.

Collision cross sections for species considered in this study are presented in figure 1. Air species cross sections range from  $1.7 \times 10^{-16} \text{ cm}^2$  to  $1.4 \times 10^{-15} \text{ cm}^2$ , approximately an order of magnitude of variation with the exception of the small species argon. The species HCN,  $H_2O$ ,  $CO_2$ , and H have large cross sections compared to air species, therefore small concentrations of these molecules in an air mixture can significantly affect the collision frequency of the mixture.

Collision frequencies calculated for this parametric study are presented in figures 2 to 6. Each figure presents calculations at a single constant pressure, and each curve depicts collision frequency at a particular constant ablator mass fraction as a function of temperature. These curves appear similar in shape from one pressure to the next. The curves shift upward in collision frequency as pressure is increased. Perhaps the most startling result of this study is the erratic variation of collision frequency with the mass fraction of phenolic carbon in the contaminated air mixture. This variation is further illustrated in figure 7 where collision frequency is plotted at constant pressure and temperature to give a mass fraction dependent graph.

Particle concentrations in the gaseous mixture and corresponding electron collision cross sections can explain the collision frequency variations in figures 2 to 7. Particle concentrations are plotted for mixtures at pressures of 1 atmosphere and 5 atmospheres for temperatures of 3135°R and 8360°R in figures 8 to 11. The collision cross sections of figure 1 are used in conjunction with these particle concentrations to illustrate the dependence of collision frequency on these variables.

The curves of particle density versus ablator mass fraction (figures 8 to 11) shift upward with increased pressure, but appear similar in shape for pressures of 1 and 5 atmospheres at constant temperature. This upward shift and similarity plus the assumption that collision cross sections are not pressure dependent explain the upward shift and the similarity of the collision frequency curves. However, the shape of the curves in figures 2 to 6 are not identical. The fact that the particle mole fractions are weakly pressure dependent can be seen in figures 8 to 11 that show slight variations in curve shapes at constant temperature with variation in pressure. These slight variations are reflected in the collision-frequency figures. For instance, the frequency curves for mass fractions of 40 and 50 percent have maxima with peaks that shift from approximately 6500°R to 7800°R as pressure is increased from 0.1 atmospheres to 5 atmospheres. Figure 12 is presented to show that this shift is due to a shift in the mole fraction of the large cross-section molecule HCN.

The erratic variation of collision frequency with ablator mass fraction can be related to the particle concentrations of three large cross-sections molecules: HCN, H<sub>2</sub>O, and CO<sub>2</sub>. Figure 7 shows two maxima in the collision frequency curves at a temperature of 3135°R. Figures 8 and 10 show that the lesser of the two peaks corresponds to peaks in the concentrations of H<sub>2</sub>O and CO<sub>2</sub>, while the larger

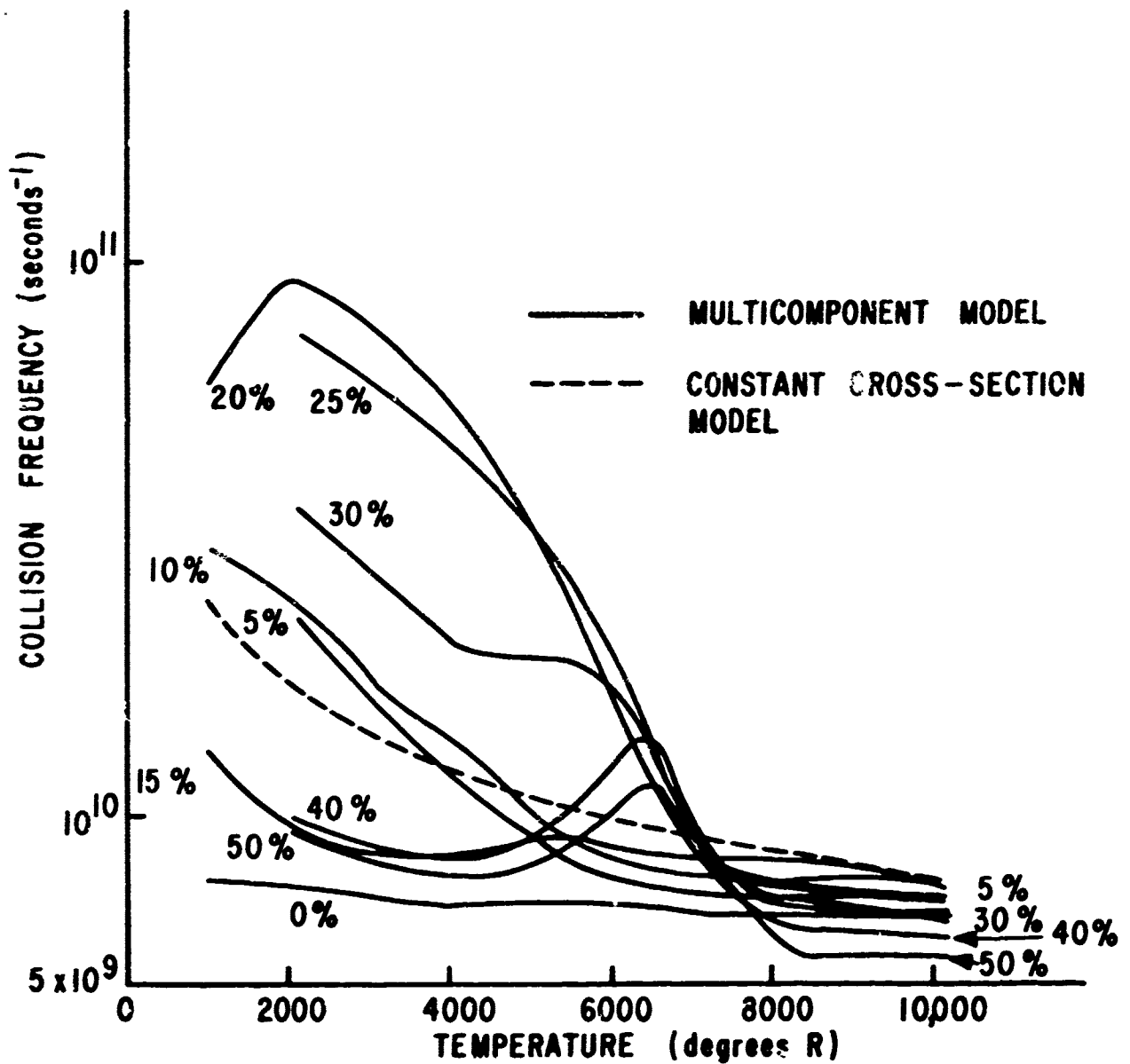


Figure 2. Parametric Study--Collision Frequency at 0.1 Atmospheres Pressure with Mass Fraction of Ablator Varying from 0 to 50 Percent

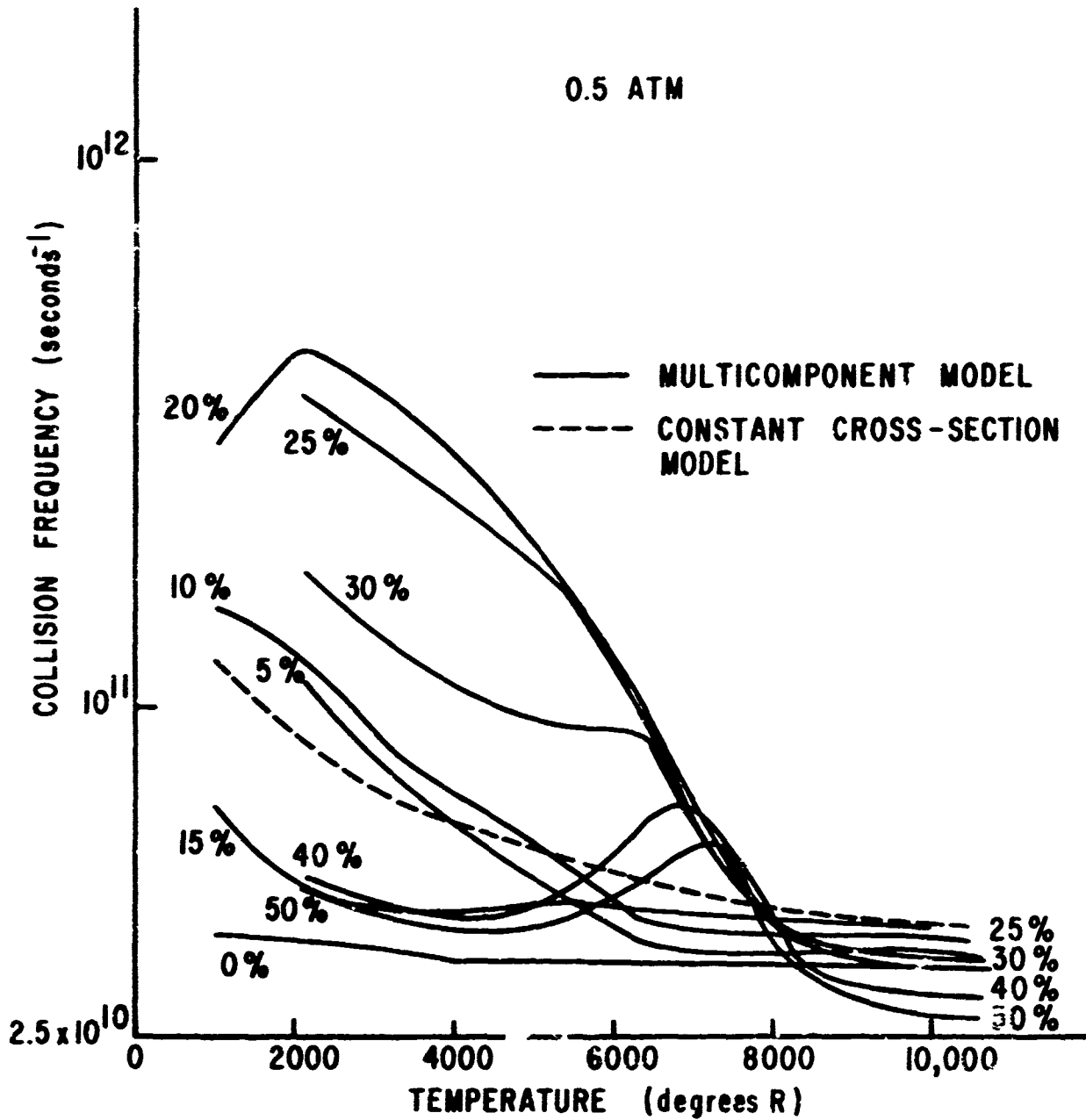


Figure 3. Parametric Study--Collision Frequency at 0.5 Atmospheres Pressure with Mass Fraction of Ablator Varying from 0 to 50 Percent

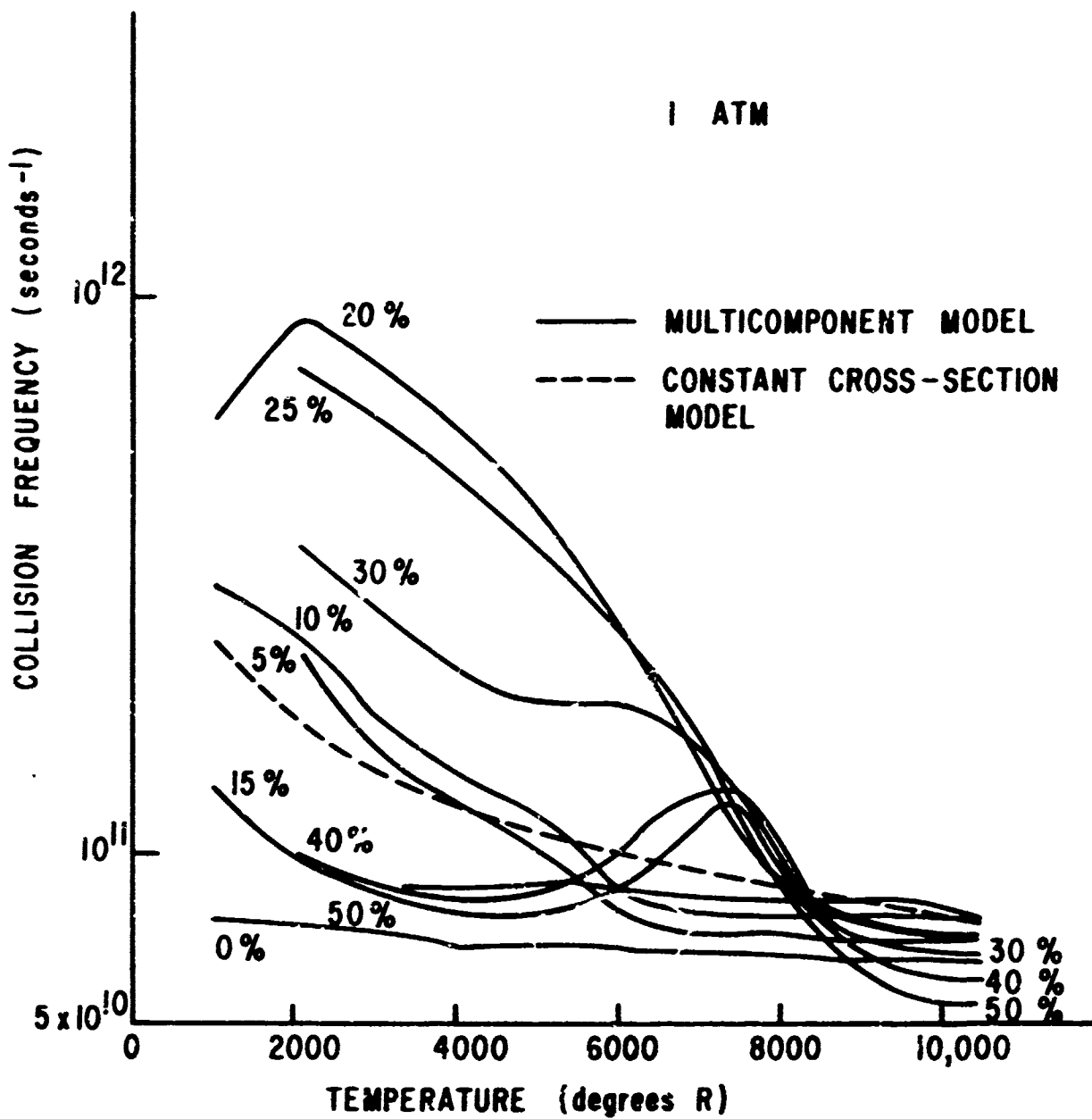


Figure 4. Parametric Study--Collision Frequency at 1.0 Atmospheres Pressure with Mass Fraction of Ablator Varying from 0 to 50 Percent

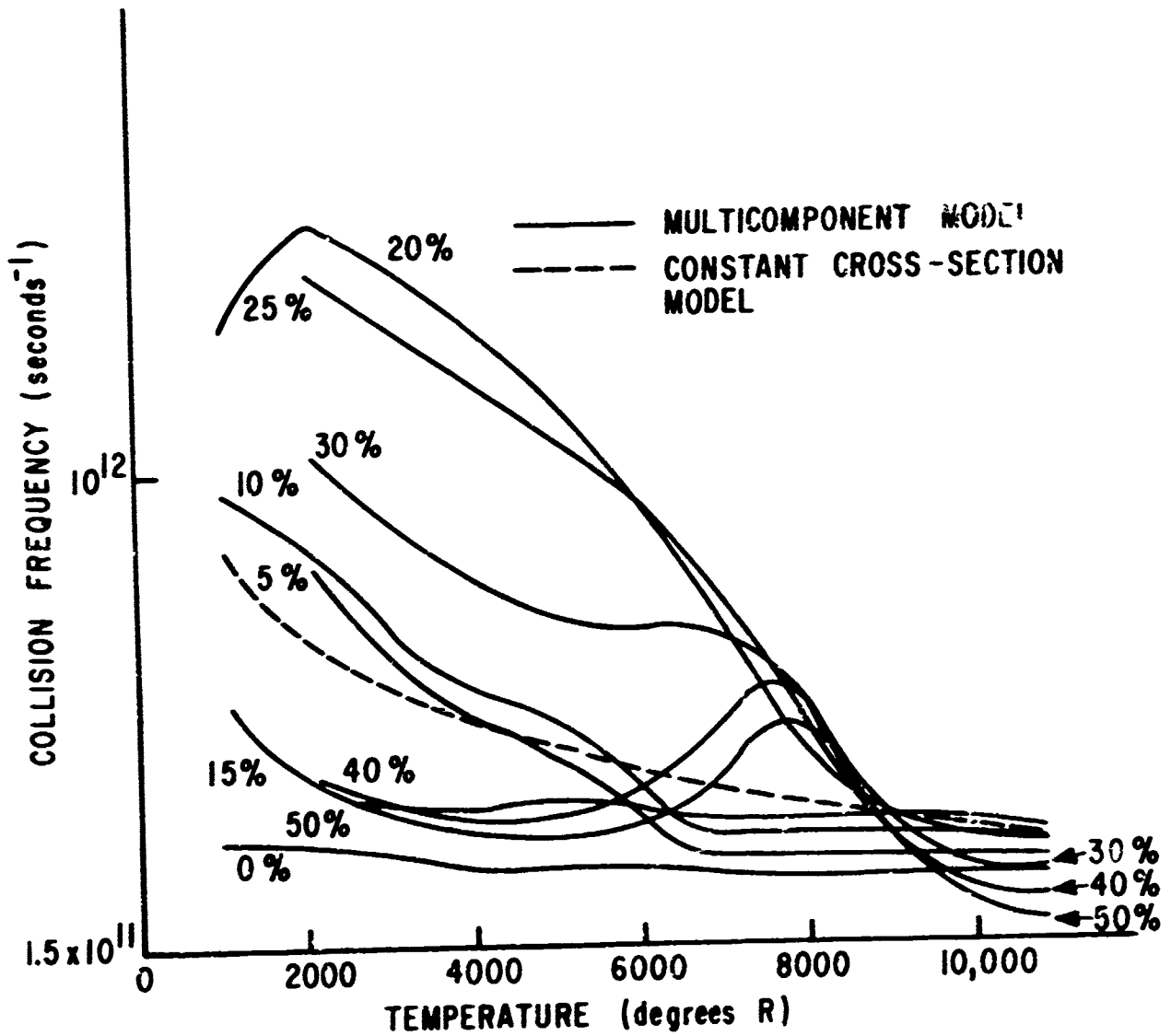


Figure 5. Parametric Study--Collision Frequency at 3.0 Atmospheres Pressure with Mass Fraction of Ablator Varying from 0 to 50 Percent

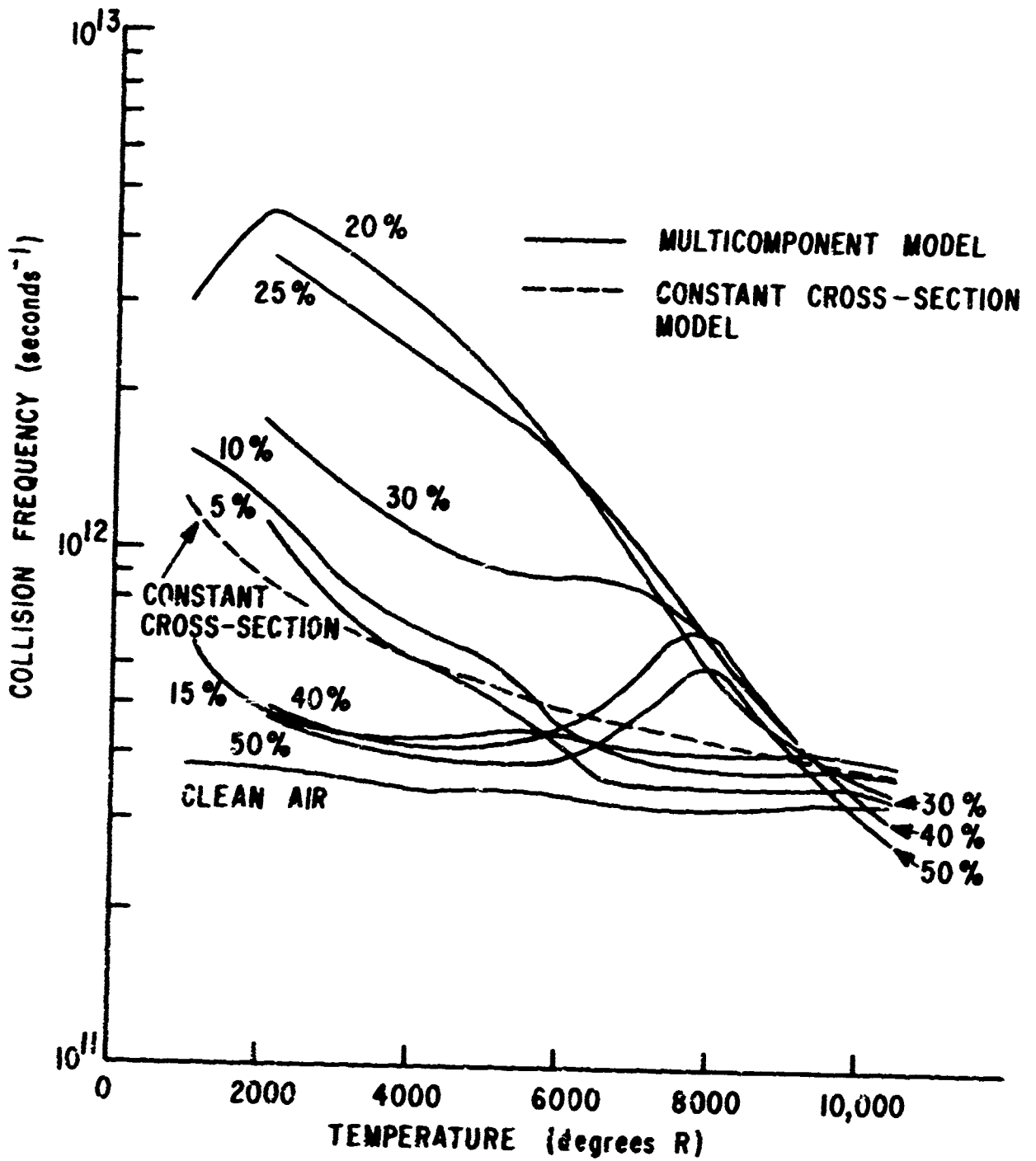


Figure 6. Parametric Study--Collision Frequency at 5.0 Atmospheres Pressure with Mass Fraction of Ablator Varying from 0 to 50 Percent

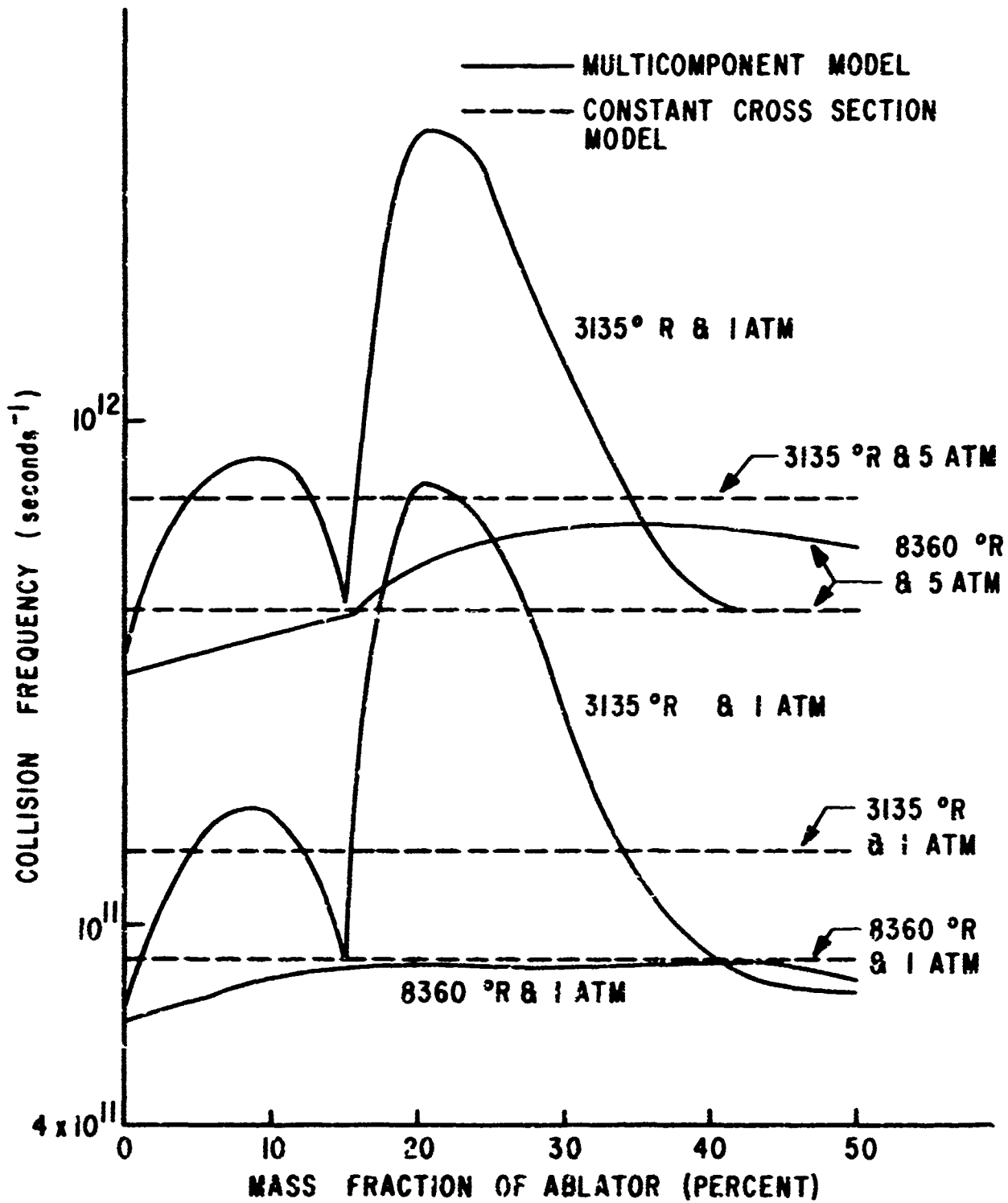


Figure 7. Parametric Study--Collision Frequency at Varying Ablator Mass Fraction with Temperature and Pressure Held Constant

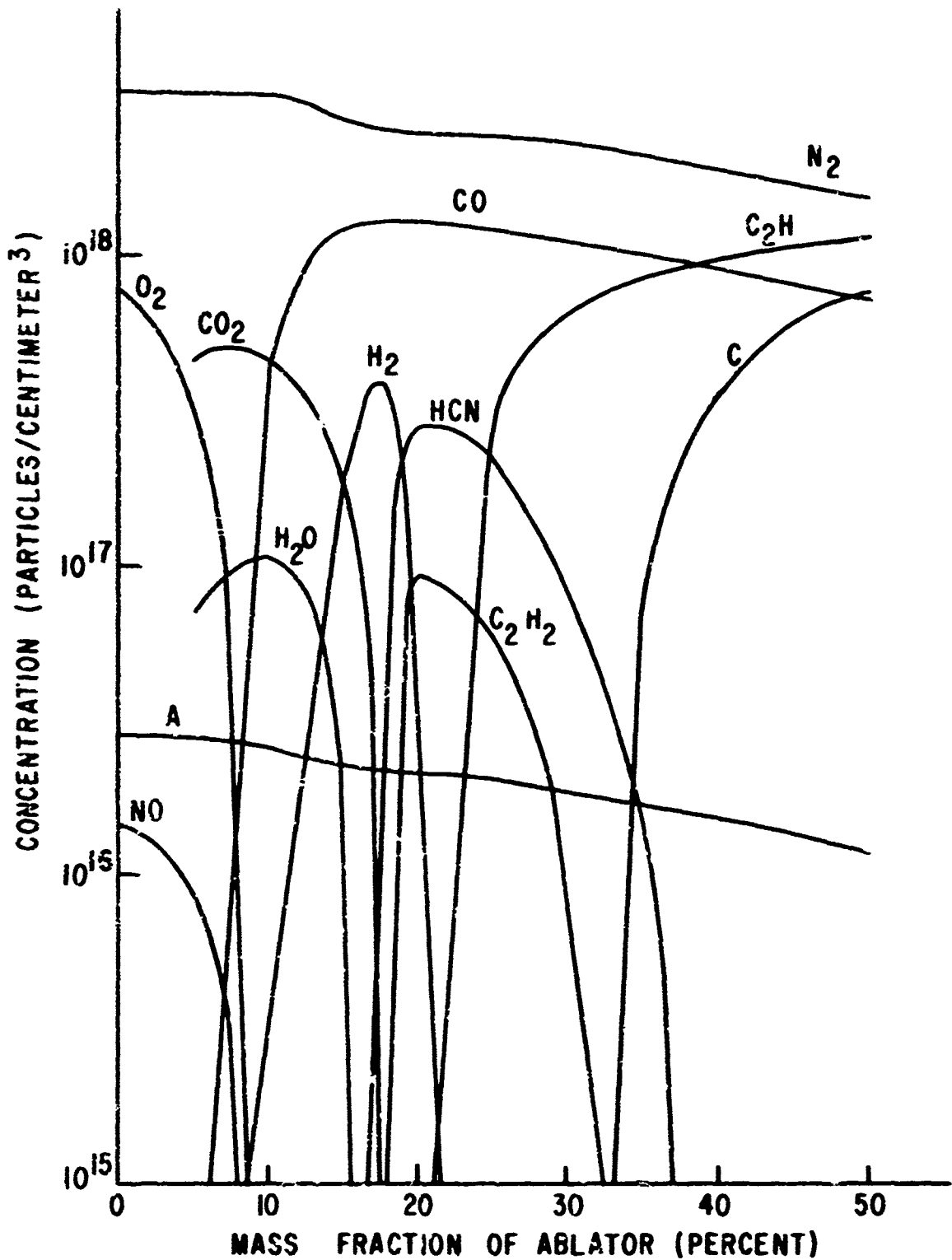


Figure 8. Parametric Study--Mixture Composition at Varying Ablator Mass Fraction at 1.0 Atmosphere Pressure and 3135°R Temperature

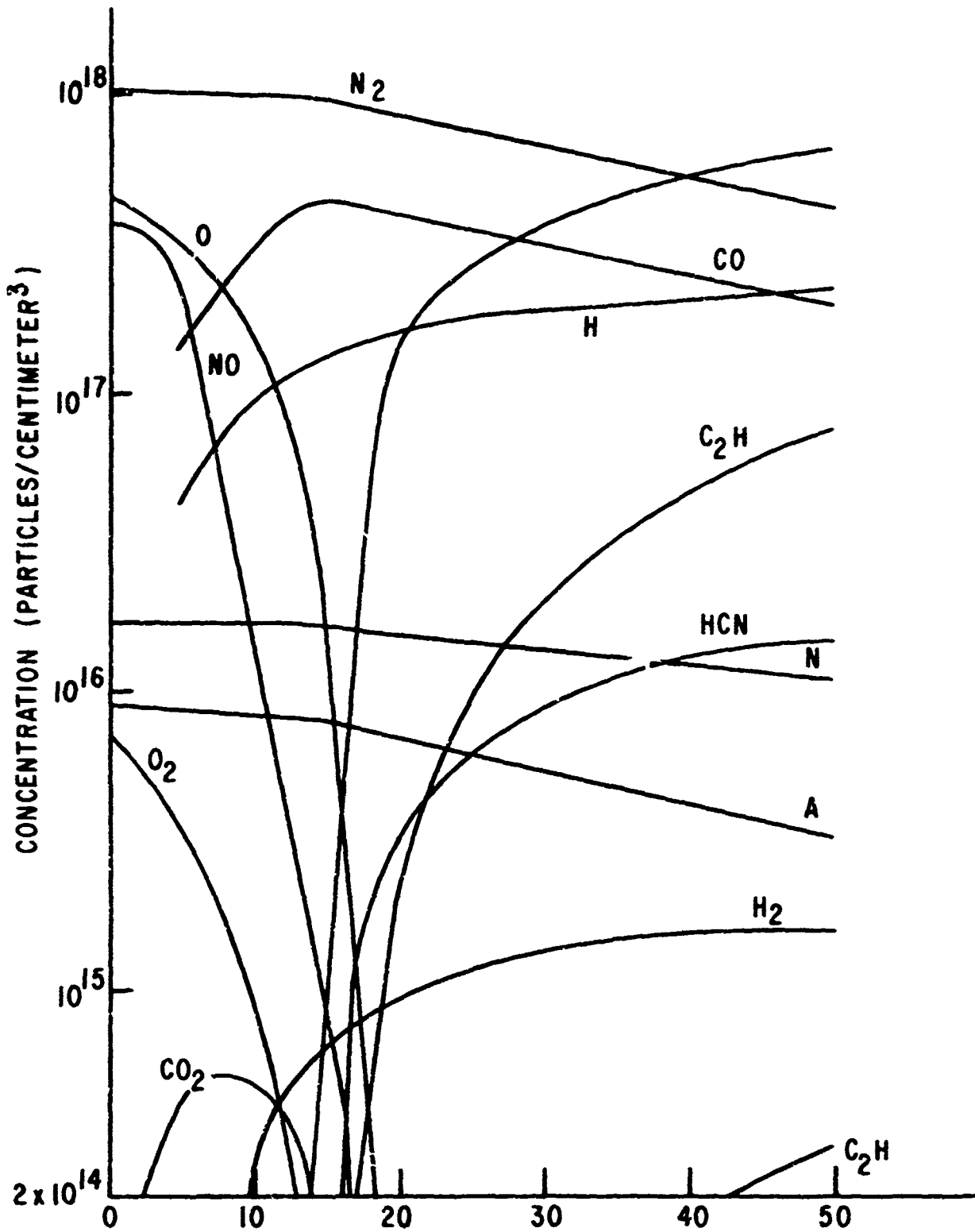


Figure 9. Parametric Study--Mixture Composition at Varying Ablator Mass Fraction at 1.0 Atmosphere Pressure and 8360°R Temperature

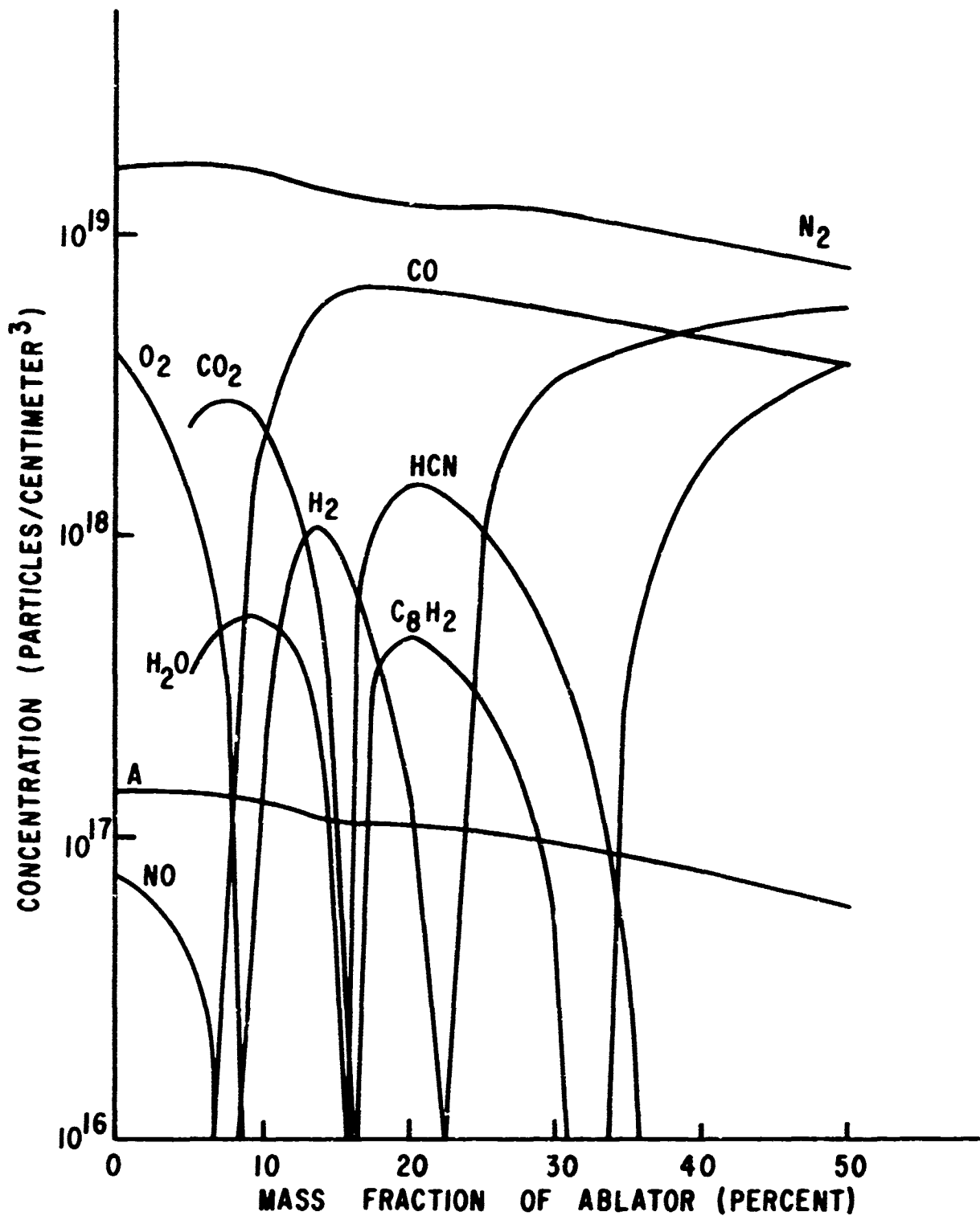


Figure 10. Parametric Study--Mixture Composition at Varying Ablator Mass Fraction at 5.0 Atmospheres Pressure and 3135°R Temperature

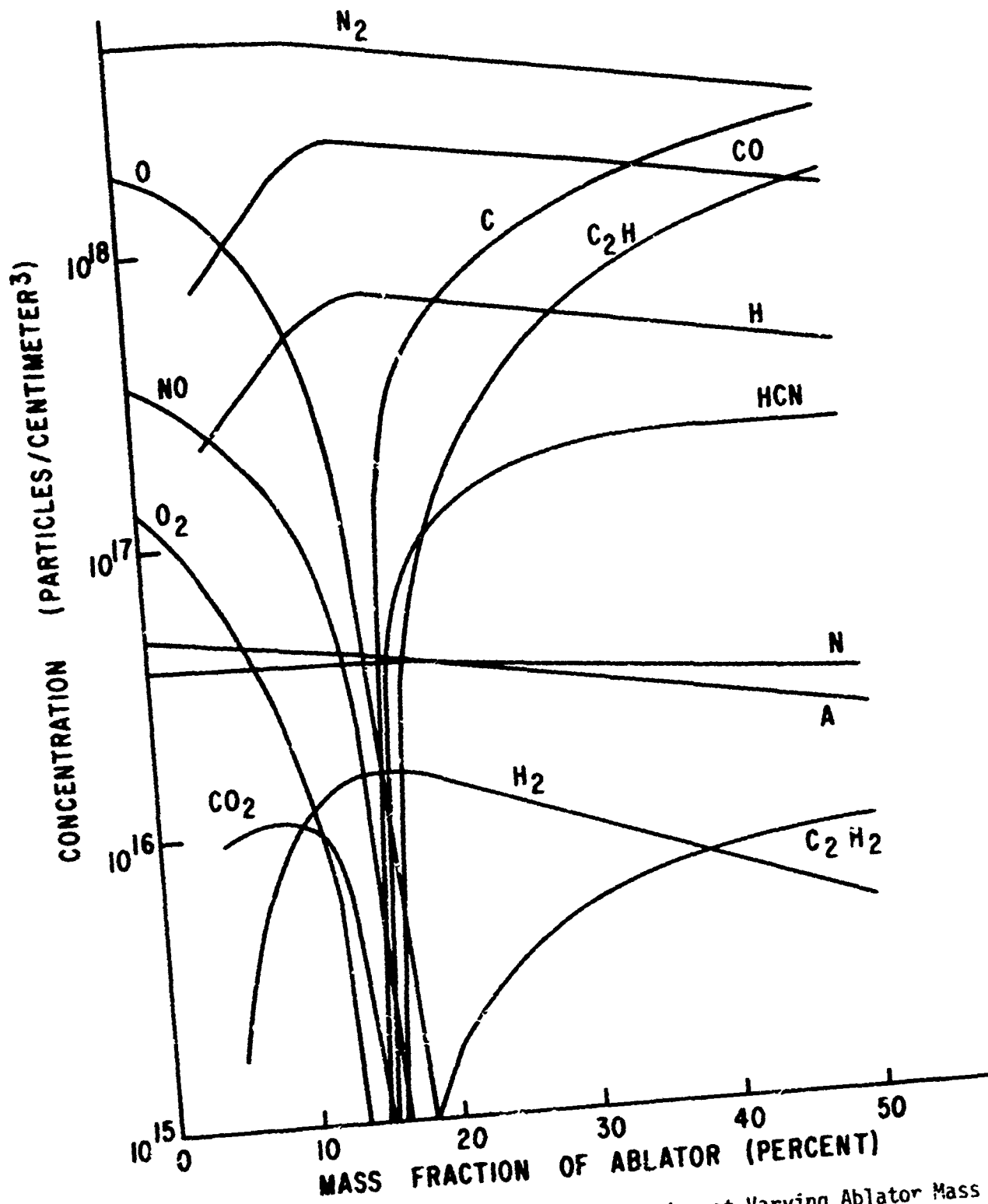


Figure 11. Parametric Study--Mixture Composition at Varying Ablator Mass Fraction at 5.0 Atmospheres Pressure and 8360°R Temperature

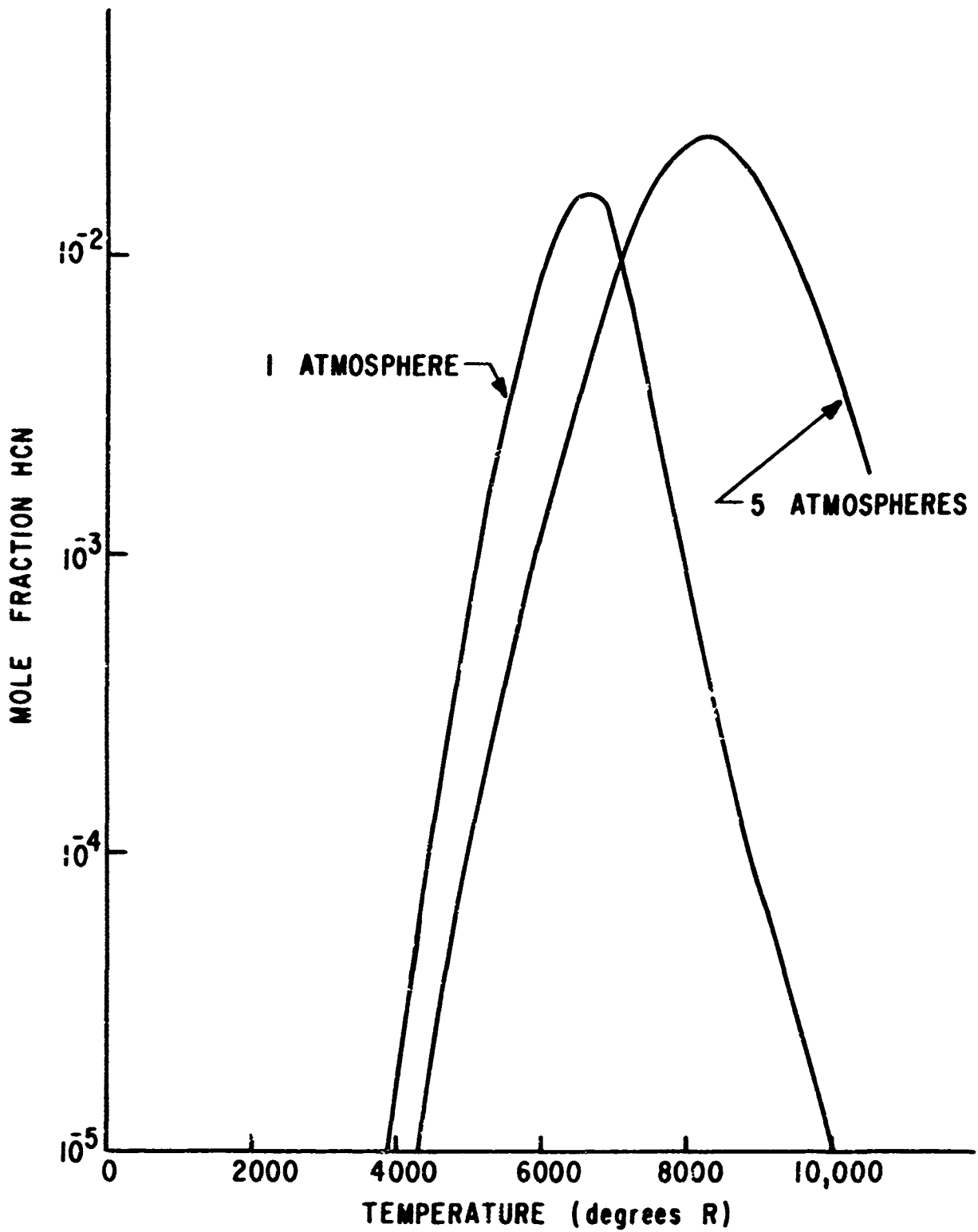


Figure 12. Parametric Study--HCN Concentration in a Mixture with an Ablator Mass Fraction of 50 Percent at Pressures of 1.0 and 5.0 Atmospheres

peak follows the concentration of HCN. At a temperature of 8360°R, the density of these molecules relative to the total density is smaller and the cross sections are much smaller. Thus, the effect of HCN, H<sub>2</sub>O, and CO<sub>2</sub> on collision frequency is small and collision frequency does not vary drastically with mass fraction at 8360°R. There is a slight increase in collision frequency at 5 atm and 8360°R. This increase corresponds to a particle density increase of HCN. The curves for 8360°R are mainly the result of superposition of collision frequencies for the N<sub>2</sub>, H, and HCN molecules.

A general trend of the collision frequency is to decrease with increasing temperature. Three factors cause this decrease. The total number density decreases with increasing temperature and the relative concentration of large cross-section molecules decreases with increasing temperature. The cross section of the large molecules HCN, H<sub>2</sub>O, CO<sub>2</sub>, and H decrease with increasing temperature. Two factors opposing this trend are the electron velocity which increases as the square root of temperature and the slight increase of the air species' cross-sections with increasing temperature.

Collision-frequency curves predicted by the constant cross-section model and by the multicomponent model are compared in figures 2 to 7. By definition the constant cross-section model cannot account for frequency variations caused by specie concentration variations at a given pressure and temperature. Therefore, the constant cross-section model predicts single curves in figures 2 to 6 and straight lines in figure 7 for varying ablator mass fraction. These figures show a factor of five maximum deviations in the collision frequencies predicted by the two models. Even for clean air the two models predict significantly different collision frequencies. The constant cross-section model predicts larger collision frequencies because the constant cross section is larger than the multicomponent collision cross sections. As temperature is increased the constant cross section and multicomponent air cross sections are more nearly equal.

SECTION IV  
STUDY OF TURBULENT BOUNDARY LAYERS

1. HIGH-VELOCITY REENTRY TRAJECTORY; CASES 1 TO 6

Collision-frequency and signal-attenuation analyses were performed for six points on a typical hypersonic reentry trajectory. The reentry vehicle studied was a sphere-cone with a 1/2-inch nose radius and an 8-degree half-angle afterbody. The afterbody heatshield was phenolic carbon with an assumed sodium contamination level of 100 ppm. A nose cap material was not assumed since the solution method could take into account only one wall material. The body station studied was 56.35 streamwise inches from the stagnation point. The six trajectory cases considered are listed in table 1.

Table I  
REENTRY TRAJECTORY

Case	Altitude (feet)	Velocity (ft/sec)
1	74,820	22,340
2	52,530	21,800
3	25,930	20,040
4	16,080	18,870
5	11,390	18,190
6	6,870	17,470

The boundary layer chemical species and electron concentration profiles required for the collision frequency and signal attenuation analyses were obtained from the AFWL similar turbulent boundary layer computer code REBOUND, (ref. 1). Boundary layer profiles of velocity, enthalpy, and ablator mass fraction are obtained by this program using the Crocco similarity assumptions. The boundary layer enthalpy is determined from a real gas wall and edge enthalpy applying the Crocco enthalpy profile. Species concentrations are determined from pressure, enthalpy, and ablation mass fraction by assuming that the gaseous mixture is in

chemical equilibrium. For a given thermodynamic state, the chemical equilibrium composition is determined by minimization of the Gibb's free energy.

The results of the boundary layer analyses are presented in figures 13 to 24. Collision frequencies calculated using the multicomponent and constant cross-section models are compared in figure 13 to 18. Temperature profiles are presented in figure 19 and ablator mass fraction profiles are presented in Figure 20. Species concentration profiles for case 3 are shown in figure 21. The electron density profiles for the six cases are shown in figure 22. The boundary layer one-way signal attenuation for the six cases is shown in figures 23 and 24.

Both the multicomponent and constant cross section models predict collision frequency profiles which appear similar for each of the six trajectory cases. As a general trend, the collision frequency curves shift upward with decreasing altitude. This is the result of increased boundary layer density with decreased altitude. An examination of the temperature and specie concentration figures can explain the shape and similarity of the curves.

Recalling equation 8 and the fact that pressure is constant across a boundary layer, it is observed that the constant cross section collision frequency is inversely proportional to the square root of the temperature. This relationship is depicted by the collision frequency curves (figures 13 to 18) and the temperature curves (figure 19). The frequency curves decrease from wall to approximately  $10^{-4}$  feet into the boundary layer. From  $10^{-4}$  feet to the boundary layer edge, the collision frequency increases. Figure 19 shows that the temperature increases from the wall to approximately  $10^{-4}$  feet and then decreases from  $10^{-4}$  feet to the boundary-layer edge.

Near the ablating wall the multicomponent model predicts higher collision frequencies than the constant cross-section model, but over a large portion of the boundary layer the multicomponent model predicts lower collision frequencies than the constant cross-section model. This deviation is clarified by the cross sections of the species (figure 1), the mass fraction profiles (figure 20), and the concentration profiles for case 3 (figure 21), which are typical of the six trajectory cases. The shapes of the multicomponent collision frequency profiles are dependent on temperature and species concentration, the pressure being constant. The large cross section of HCN and its number density profile, indicate that this molecule makes a large contribution to the collision frequency near the wall. In conjunction with other significant contributors such as  $N_2$ , H, and CO,

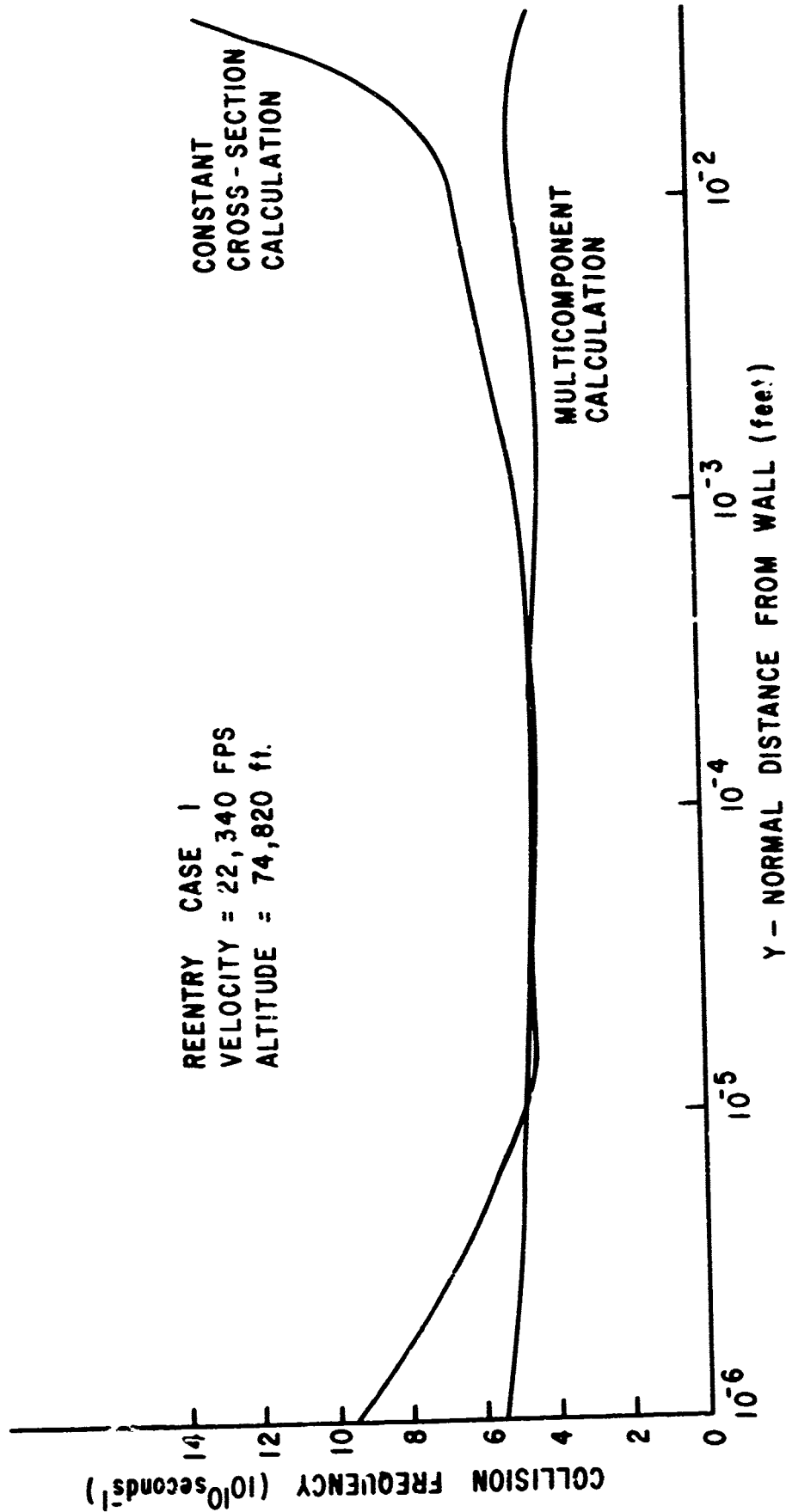


Figure 13. Reentry Trajectory Case 1--Boundary Layer Collision Frequency Profile

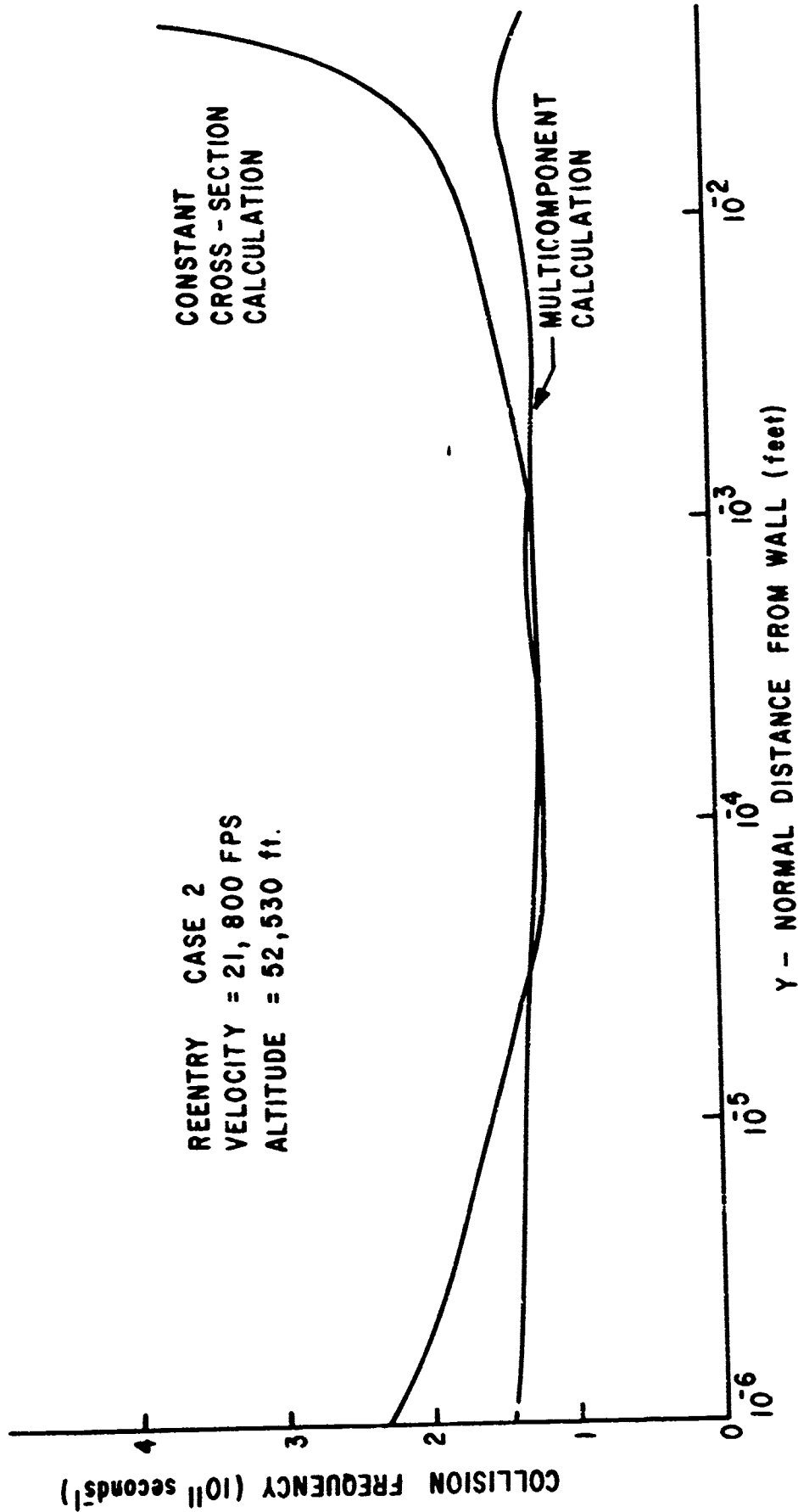


Figure 14. Reentry Trajectory Case 2--Boundary Layer Collision Frequency Profile

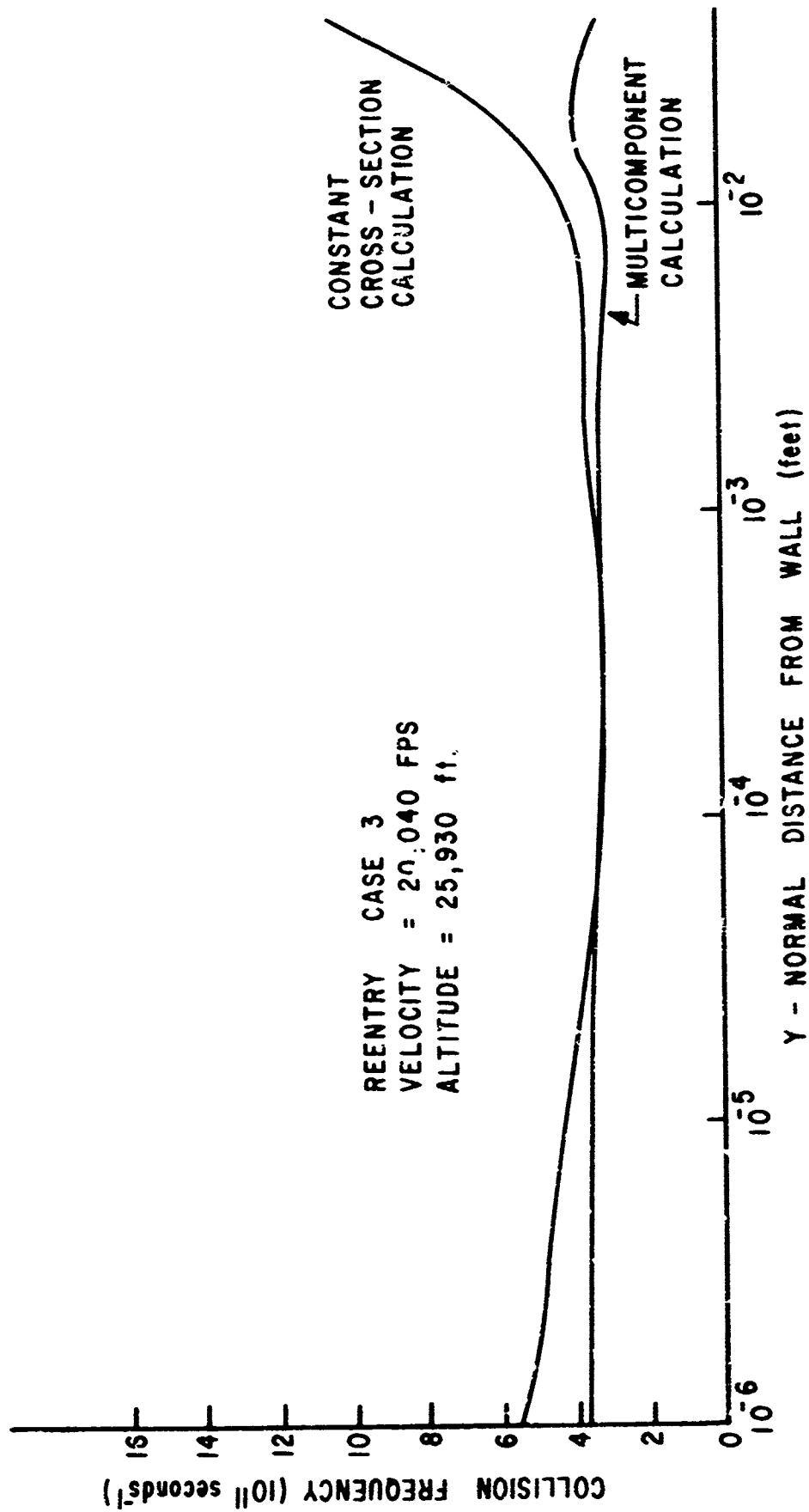


Figure 15. Reentry Trajectory Case 3--Boundary Layer Collision Frequency Profile

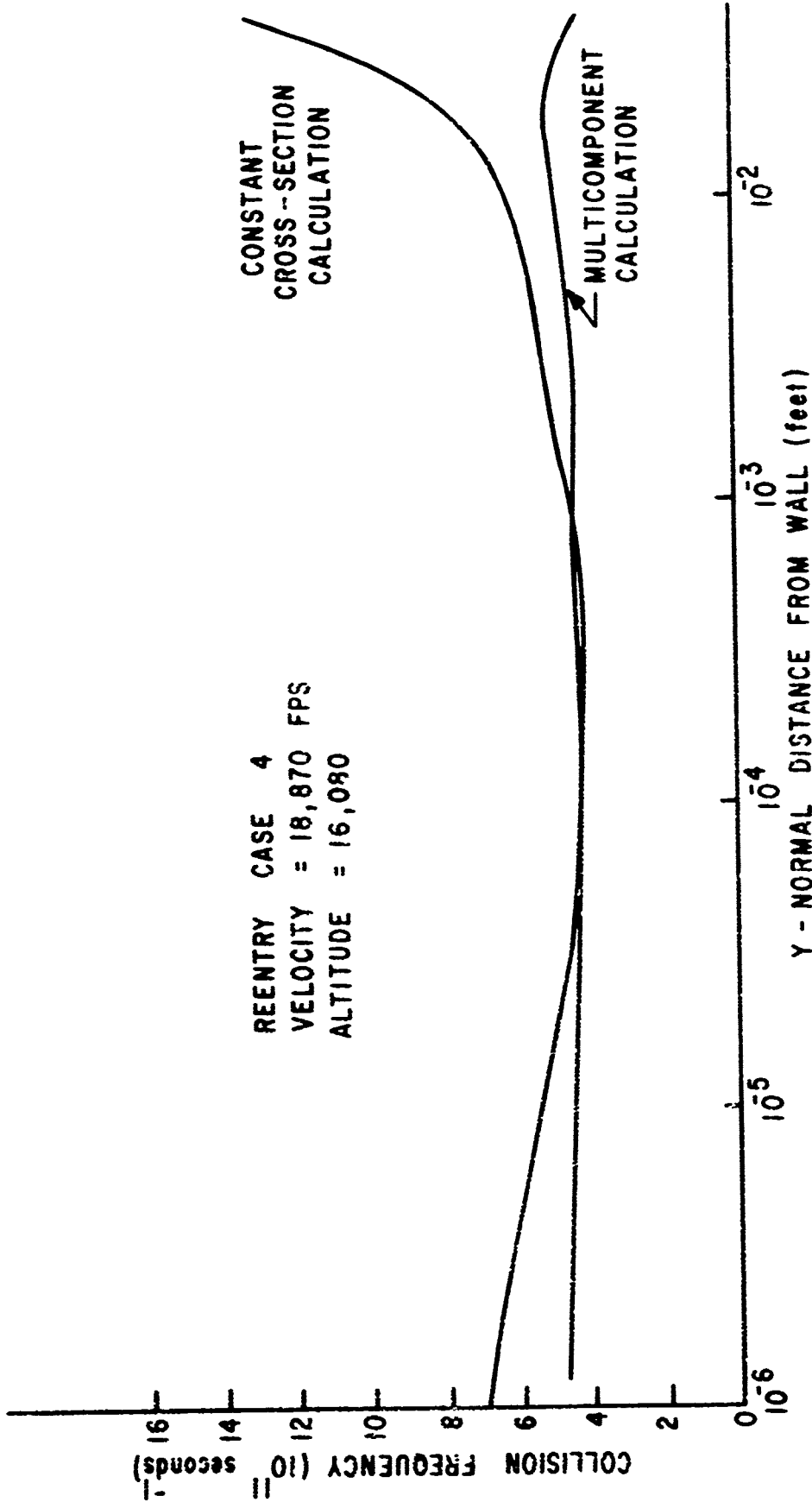


Figure 16. Reentry Trajectory Case 4--Boundary Layer Collision Frequency Profile

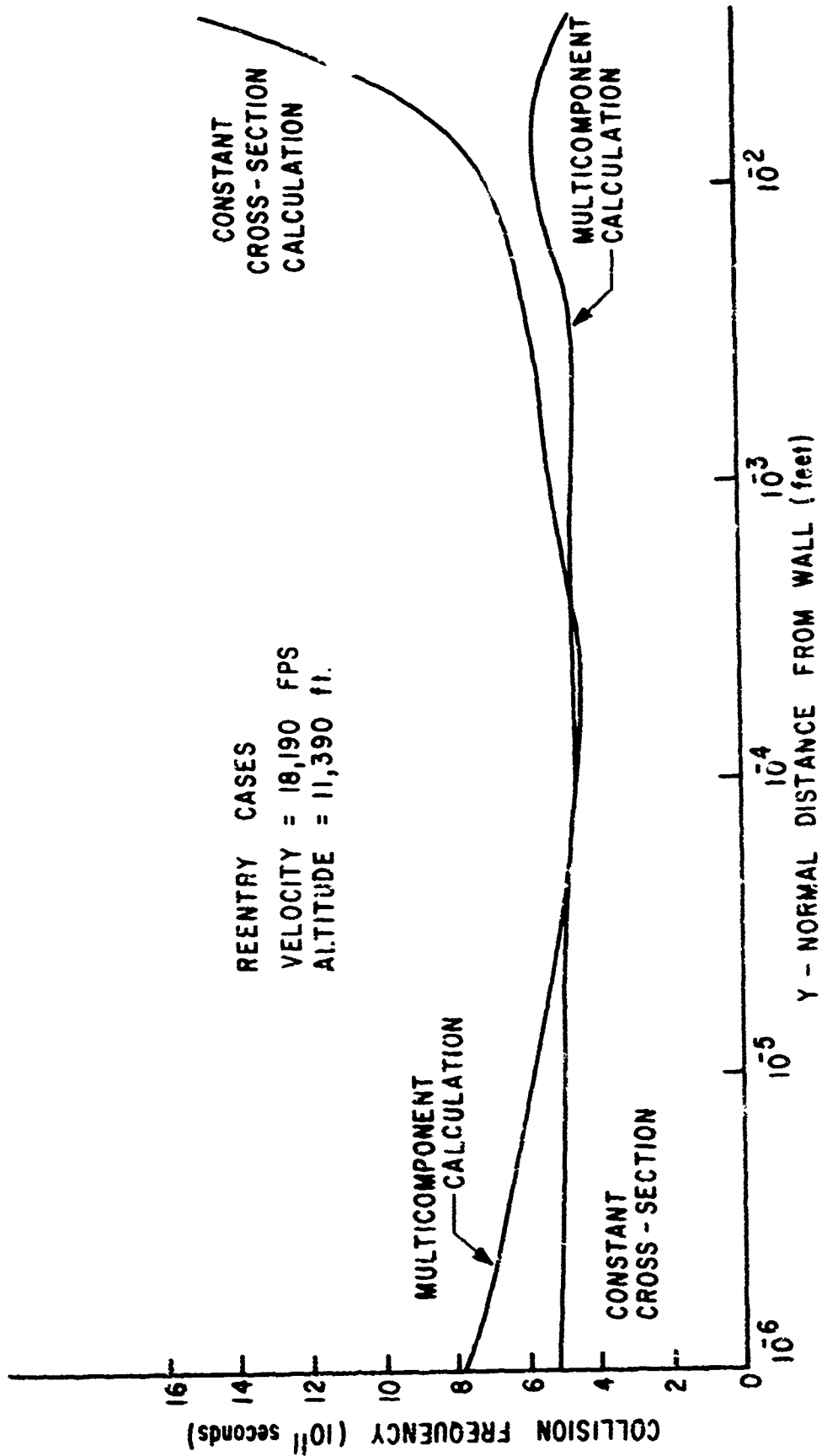


Figure 17. Reentry Trajectory Case 5--Boundary Layer Collision Frequency Profile

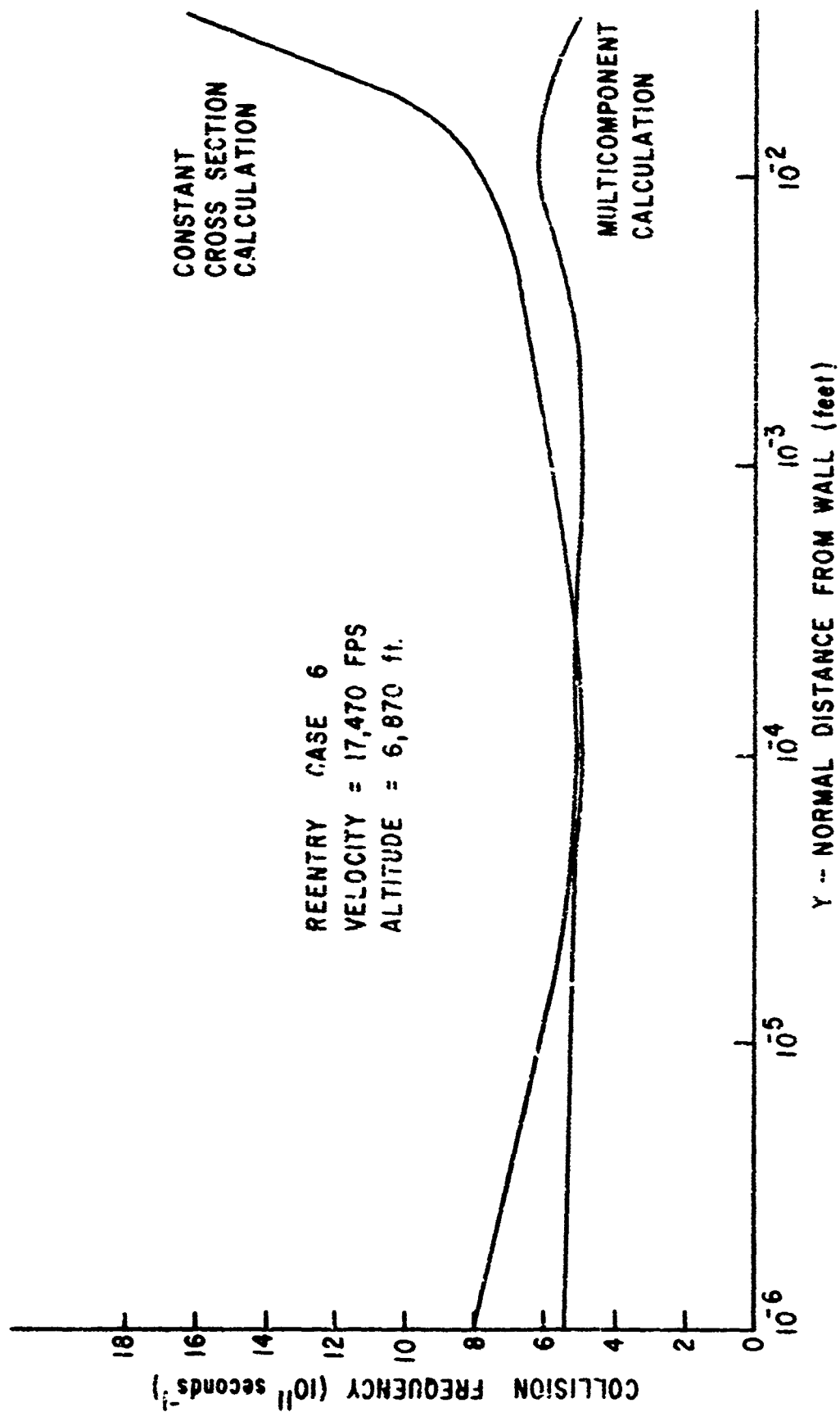


Figure 18. Reentry Trajectory Case 6--Boundary Layer Collision Frequency Profile

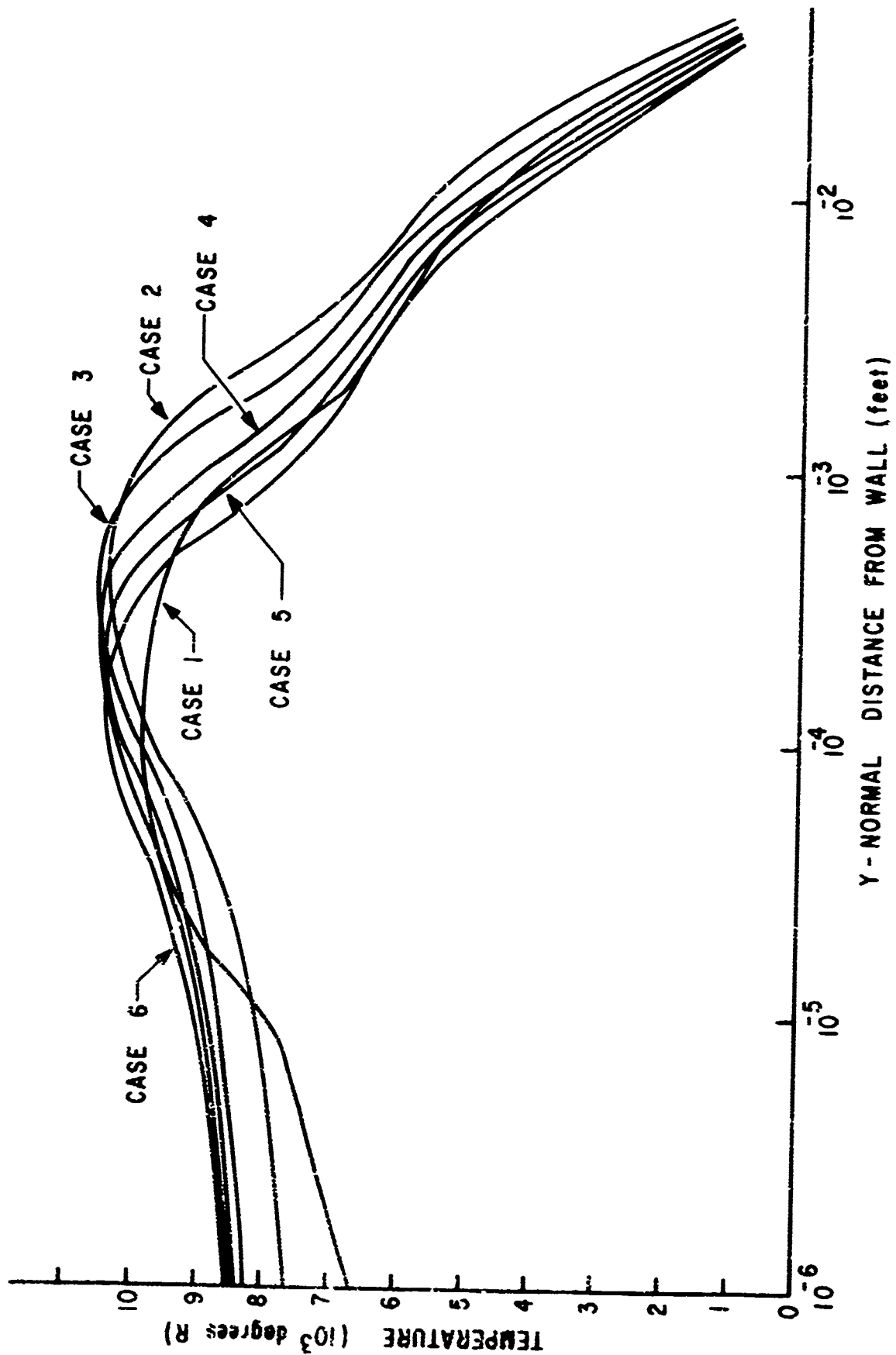


Figure 19. Reentry Trajectory Study--Boundary Layer Temperature Profile

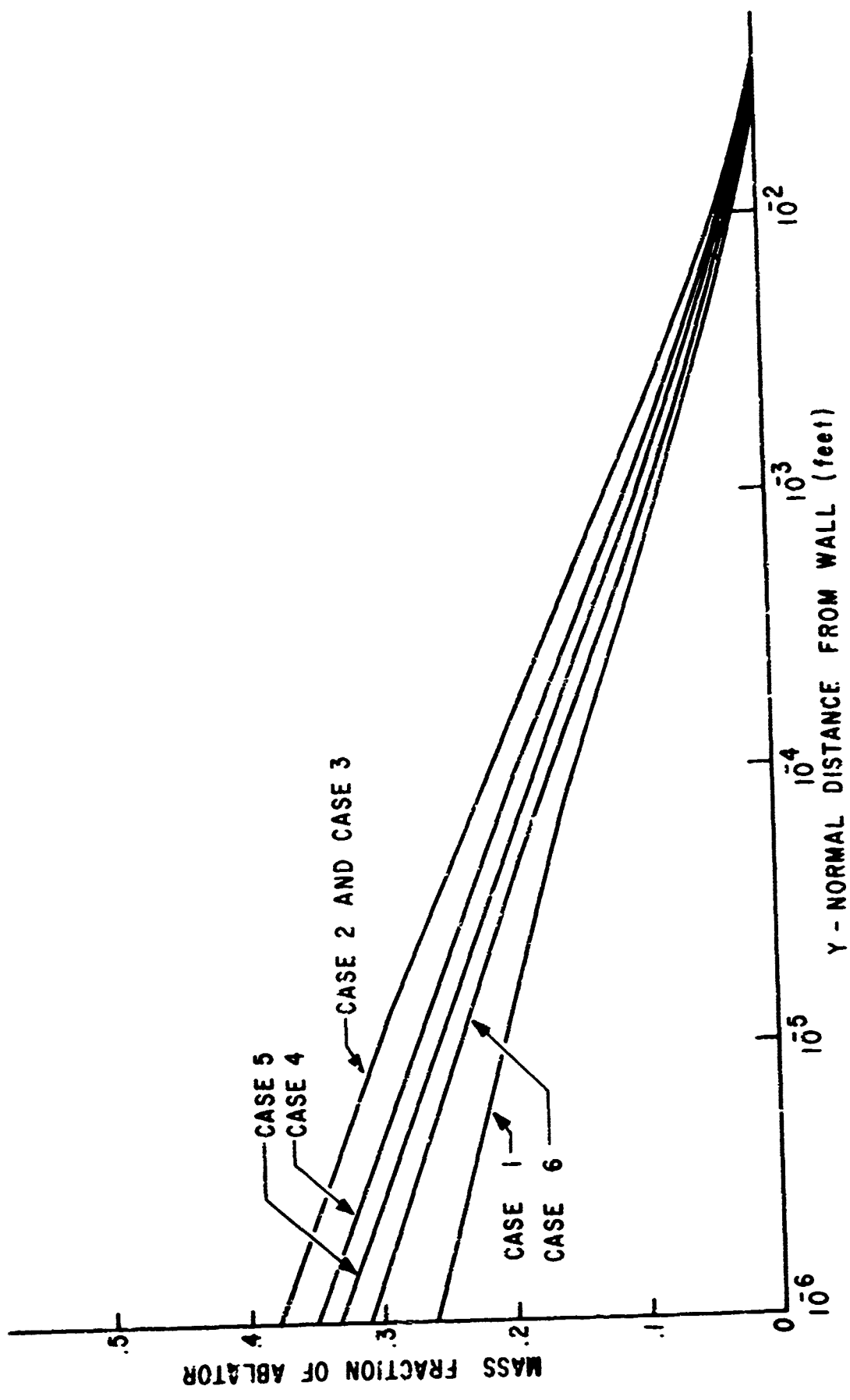


Figure 20. Reentry Trajectory Study--Boundary Layer Mass Fraction Profile

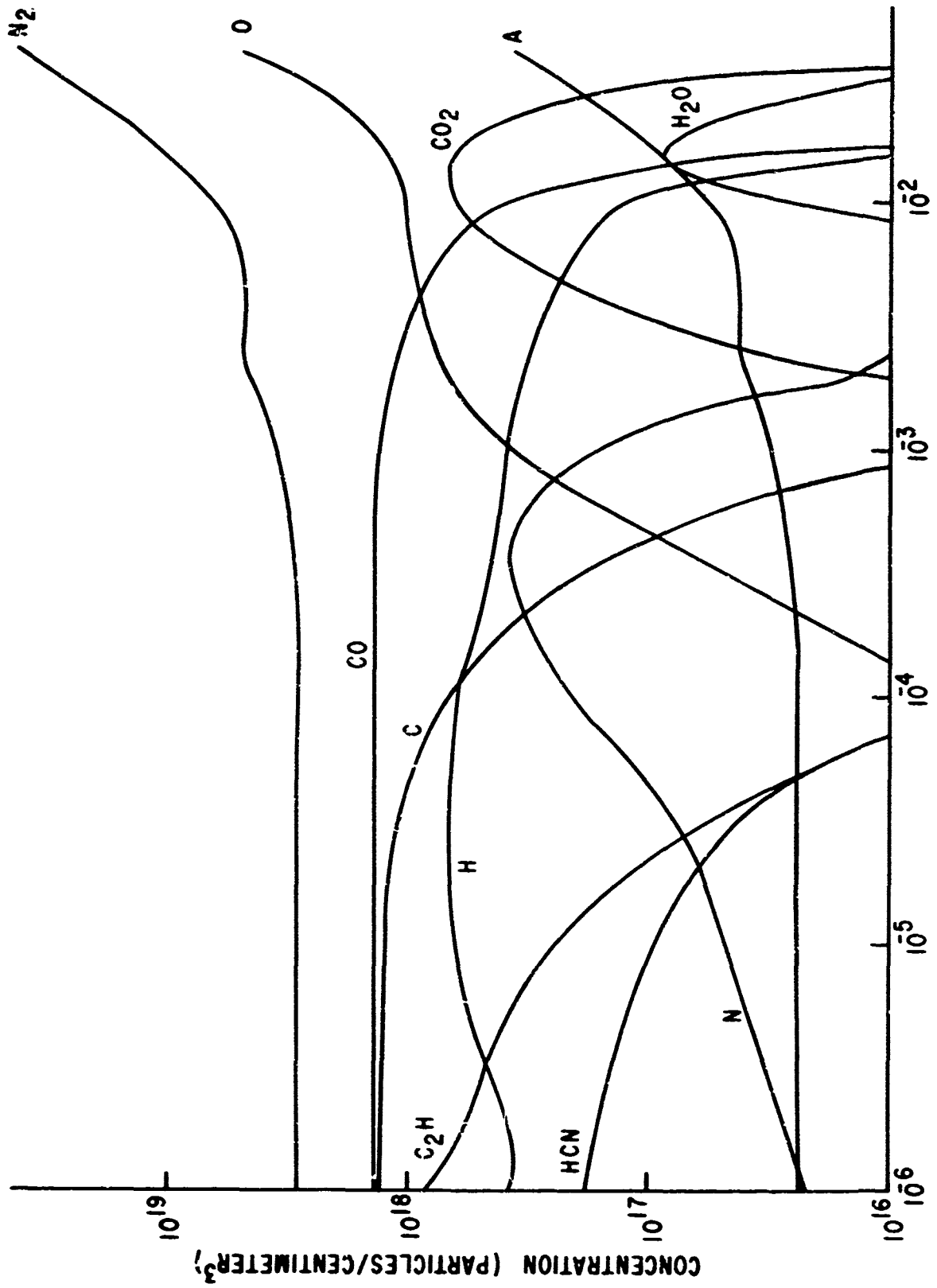


Figure 21. Reentry Trajectory Case 3--Boundary Layer Species Concentration Profiles

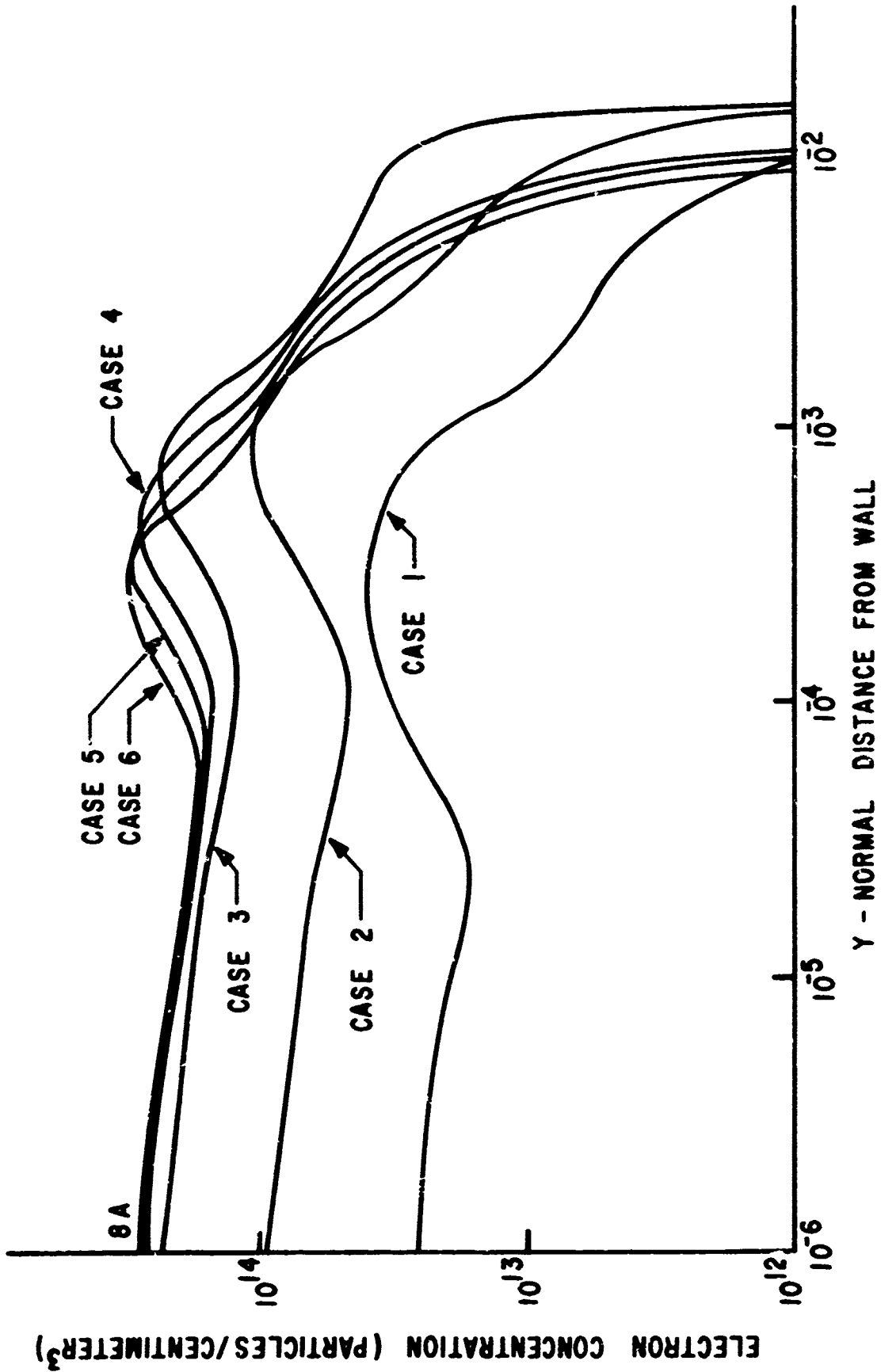


Figure 22. Reentry Trajectory Study--Boundary Layer Electron Concentration Profiles

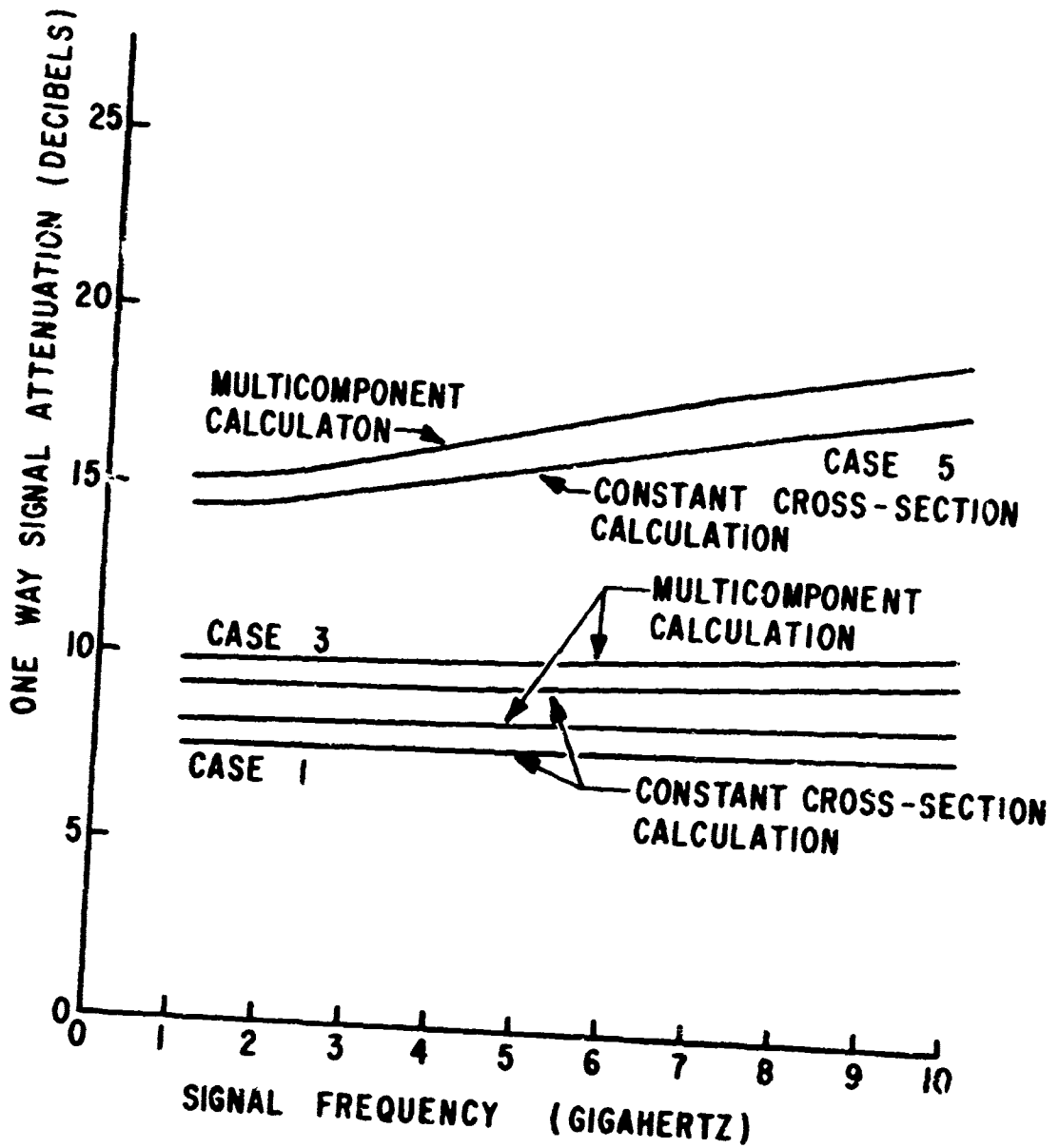


Figure 23. Reentry Trajectory Study--Boundary Layer Signal Attenuation

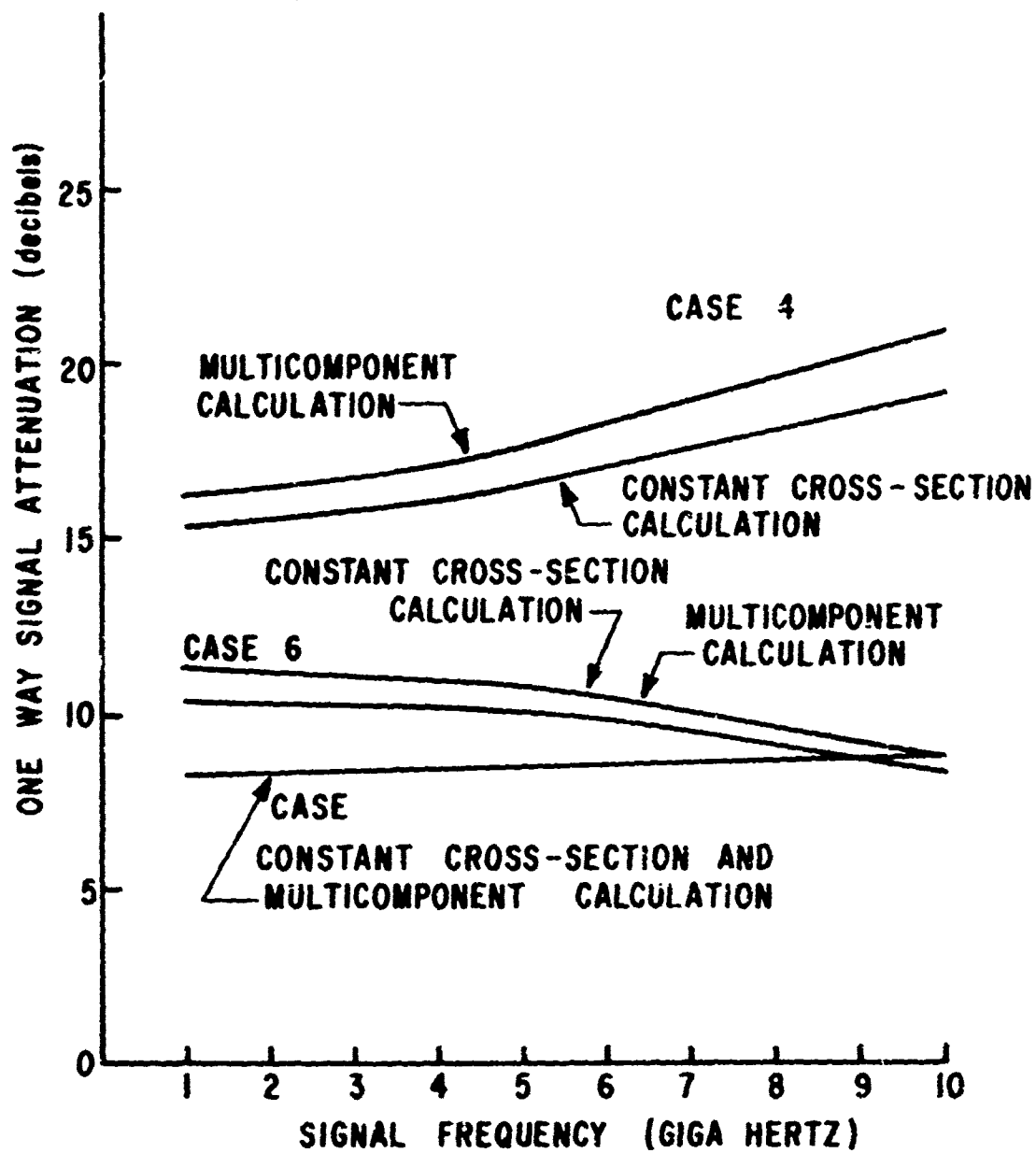


Figure 24. Reentry Trajectory Study--Boundary Layer Signal Attenuation

the HCN molecule makes the multicomponent collision frequencies greater than the collision frequencies predicted by the constant cross-section model near the wall. Over a large portion of the boundary layer the multicomponent collision frequency curve is relatively flat, in spite of an increase in total particle density towards the boundary layer edge. The mass fraction of ablation material decreases toward the boundary layer edge and the large ablation species become less significant. The multicomponent collision frequencies become lower than the constant cross-section frequencies at approximately  $10^{-3}$  feet because the temperature decreases toward the boundary layer edge and causes a decrease in the cross sections of the clean air molecules. The slight rise in the multicomponent frequency curve near  $10^{-2}$  feet corresponds to the densities of the large  $\text{CO}_2$  and  $\text{H}_2\text{O}$  molecules.

Electron densities that were obtained from chemical equilibrium calculations are presented in figure 22. Although several ionized species were included in this study, the free electrons predominately resulted from ionized sodium. Because the ablative material contains 100 ppm of sodium by weight, the mass fraction of sodium is given by the ablator mass fraction profiles multiplied by  $10^{-4}$ .

Because the amount of sodium in the boundary layer decreases from the wall to the edge in conjunction with the ablator mass fraction (figure 20), the electron density might be expected to decrease also. The electron density does decrease toward the edge, but not monotonically. The electron density is dependent on mixture composition, pressure, and temperature. It is noted that both peak temperatures and peak electron densities occur in the boundary layer region between  $10^{-4}$  and  $10^{-3}$  feet.

Signal attenuation calculations were made using the collision frequencies plotted in figures 13 to 18 and the electron densities plotted in figure 22. Comparing the multicomponent signal attenuation to the constant cross-section signal attenuation, a maximum deviation of approximately 10 percent is observed (figures 23 and 24). This signal attenuation deviation is considerably less drastic than the deviations in collision frequency of figures 13 to 18.

Equation 1 shows that the complex dielectric constant decreases as electron density increases and as collision frequency decreases. The propagation constant for the transmitted signal is proportional to the square root of the complex dielectric constant. Thus, if the plasma sheath is divided into equal slabs, the greatest signal attenuation will occur in the slabs with the largest ratio

of  $\frac{v_c \text{ Ne}}{\omega_s} / (\omega_s^2 + v_c^2)$ . Observation of the collision frequency and the electron density curves indicate why the attenuation calculations varied moderately for the two models. The largest deviation of collision frequencies occurred in two regions. The first region, from the wall to approximately  $10^{-5}$  feet, is very thin and thus had little effect on the total signal attenuation. The second region, from  $1.5 \times 10^{-2}$  feet to the edge, is relatively large but the electron density is very small and thus signal attenuation is small. Most of the signal attenuation occurred in the remaining region, from  $10^{-5}$  feet to  $1.5 \times 10^{-2}$  feet. Figure 25, which is a linear plot of the collision frequencies and electron density for case 3, clearly shows that most of the signal attenuation occurs in this region. The collision frequency deviations in this region are moderate and explain the moderate, i.e., less than 10 percent, signal attenuation deviations.

## 2. REENTRY CASE ANALYZED BY BLIMP CODE; CASE 7

Because accurate determination of chemical species concentrations is important to the multicomponent collision frequency calculations, it is appropriate to include a reentry case in which the chemistry is completely coupled to the boundary layer equations. The AFWL nonsimilar chemically reacting turbulent boundary layer computer code, BLIMP (ref. 3) solves these coupled equations. This code assumes chemical equilibrium and uses real gas properties in the flow equations. The vehicle studied for this case was a sphere-cone with a 0.238-inch nose radius and an 8-degree half-angle afterbody. The nose was graphite, and the afterbody heatshield was phenolic carbon. The heat-shield material was assumed to contain 50 ppm of sodium by weight. A streamwise station located at 3.5 feet from the stagnation point was analyzed at 85,000 feet altitude and 22,950 feet per second velocity.

Collision frequency, specie concentration, temperature, and electron density profiles are presented for this case in figures 26 to 29, respectively. The multicomponent model is seen to predict much higher collision frequencies than the constant cross-section model in the vicinity of the wall, i.e., from the wall to  $5 \times 10^{-4}$  feet. In the region from  $5 \times 10^{-4}$  feet to  $1.2 \times 10^{-2}$  feet to the edge, the collision-frequency curves diverge. An explanation of the deviation between the two models is given by the specie concentration profiles in figure 27. The shape of the constant cross-section profile is determined completely by temperature in figure 27, because pressure is constant. Significant concentrations of the large HCN, H, and CO molecules make the specie dependent

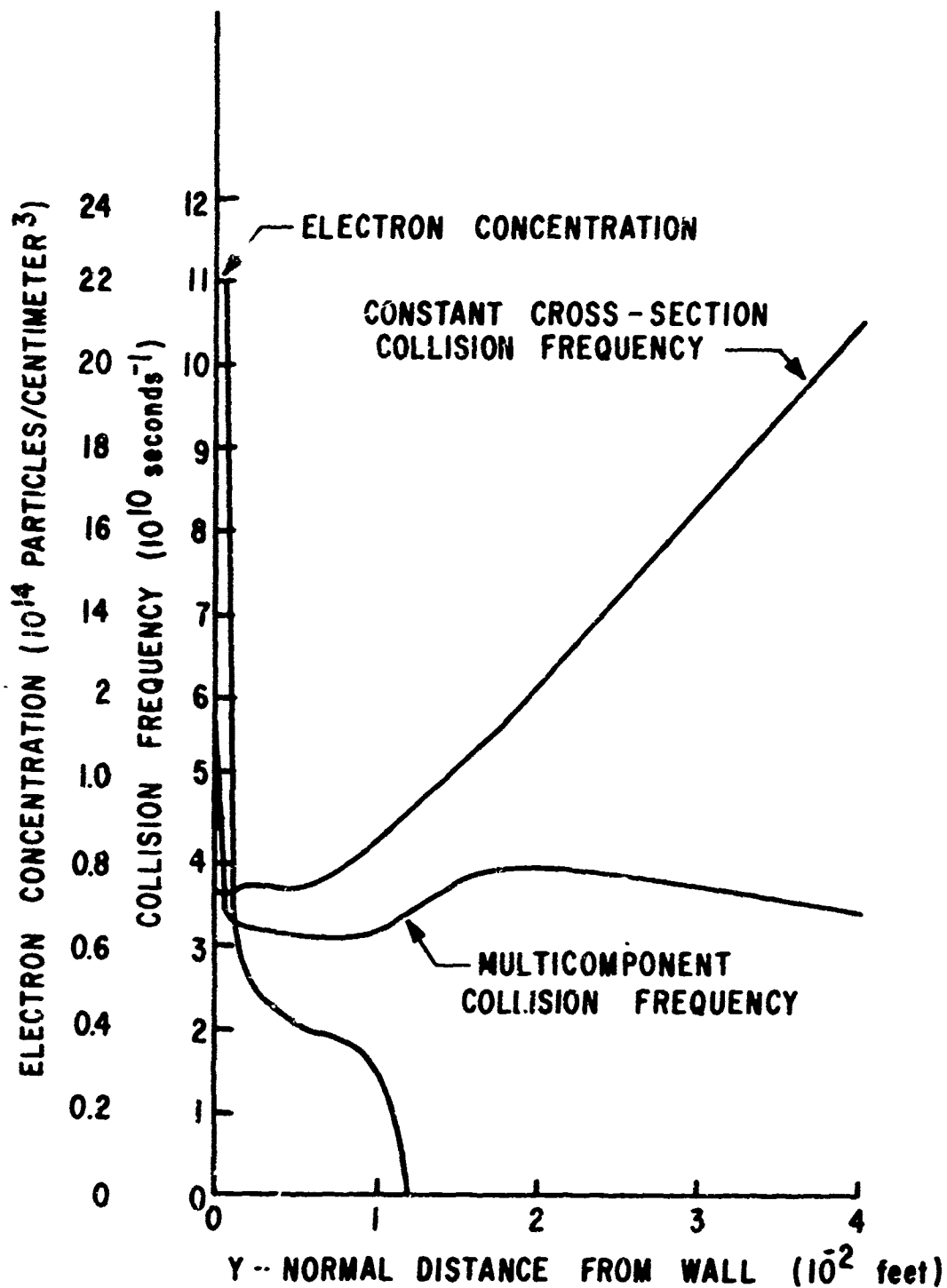


Figure 25. Reentry Trajectory Case 3--Boundary Layer Electron Concentration and Collision Frequency Profiles

CASE 7  
VELOCITY = 22,950 FPS  
ALTITUDE = 85,000 ft.

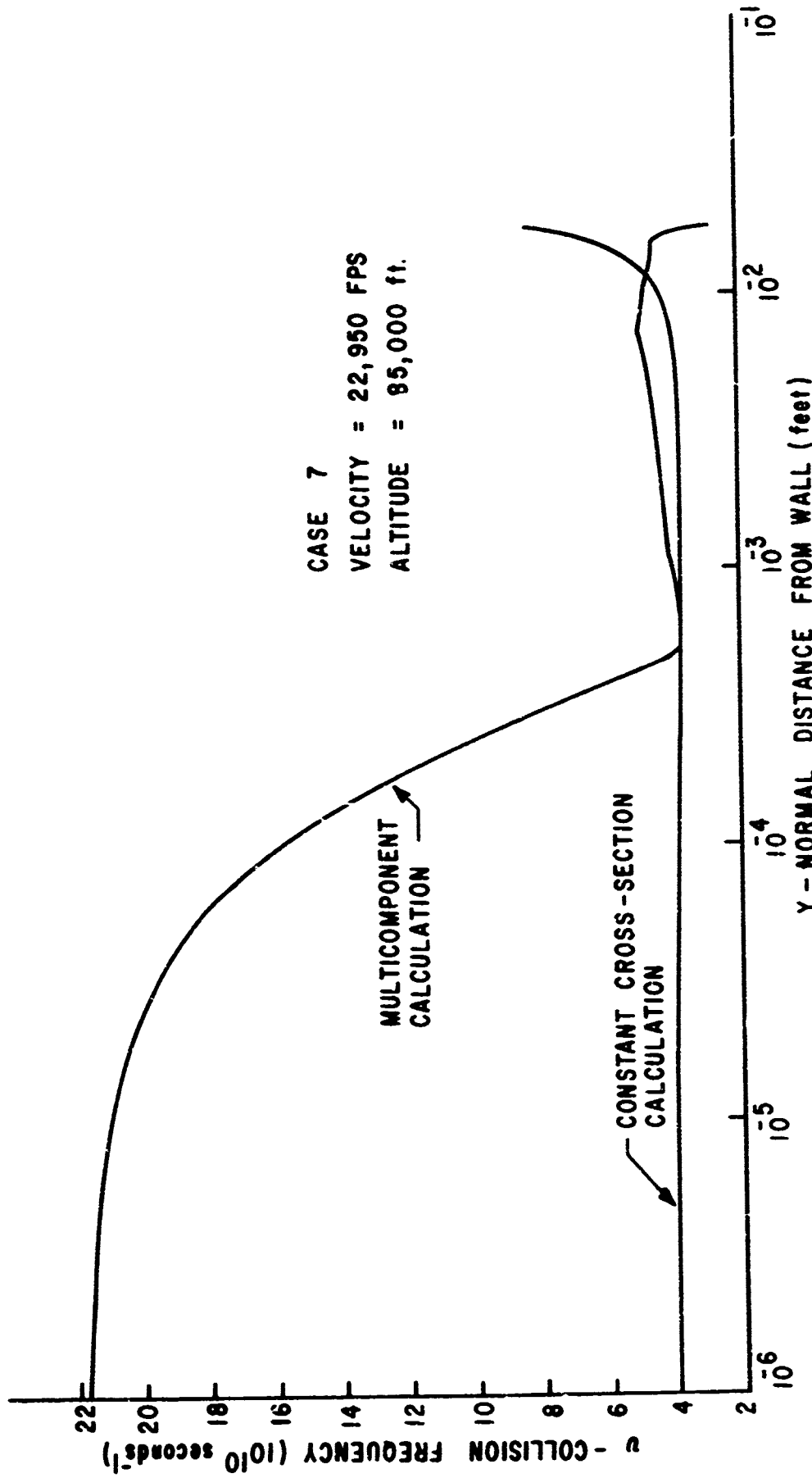


Figure 26. Nonsimilar Reentry Analysis--Boundary Layer Collision Frequency Profile

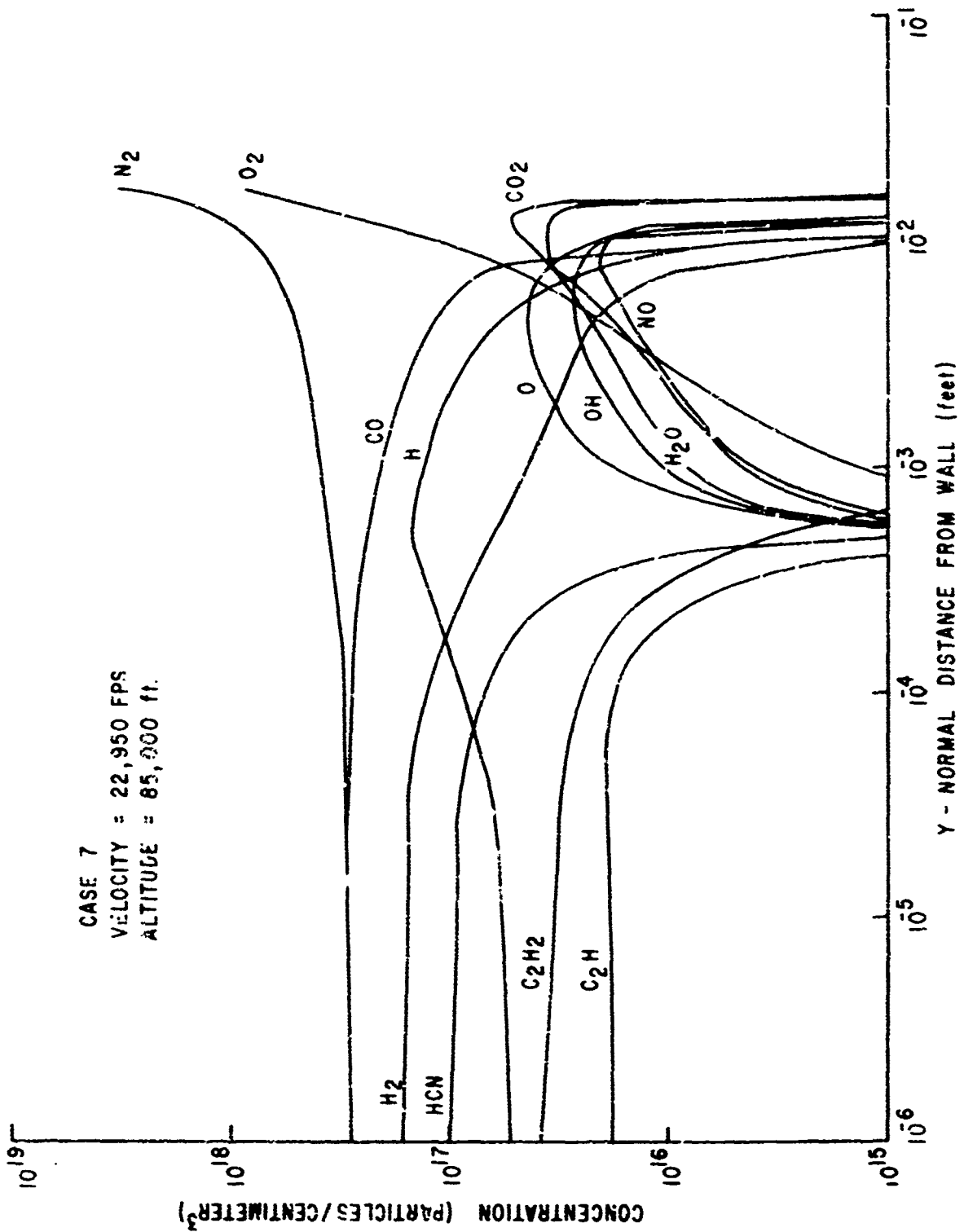
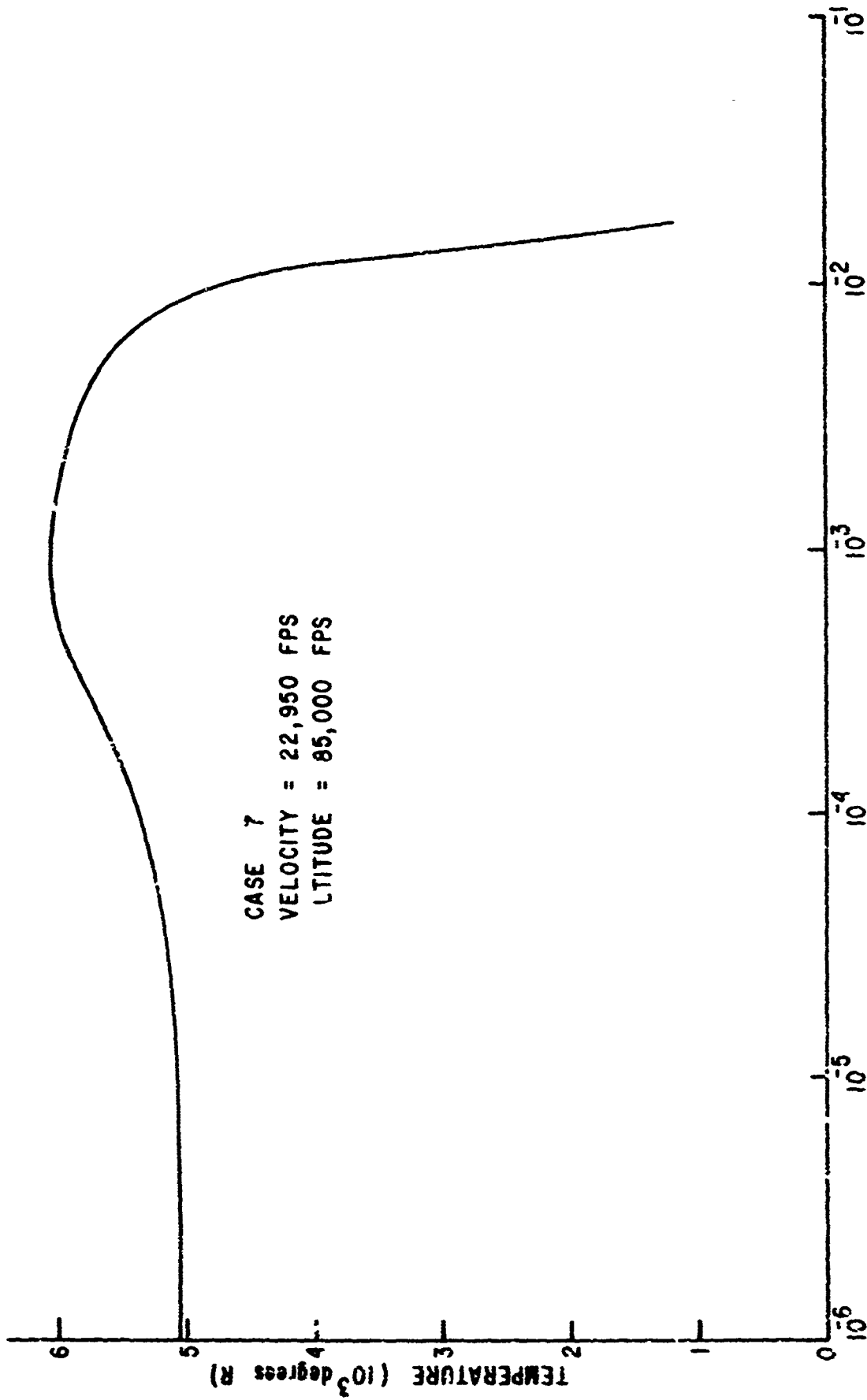


FIGURE 27. NONSIMILAR REENTRY ANALYSIS--BOUNDARY LAYER SPECIES CONCENTRATION PROFILES



CASE 7  
VELOCITY = 22,950 FPS  
ALTITUDE = 85,000 FPS

Y - NORMAL DISTANCE FROM SURFACE

Figure 28. Nonsimilar Reentry Ar. is--Boundary Layer Temperature Profile

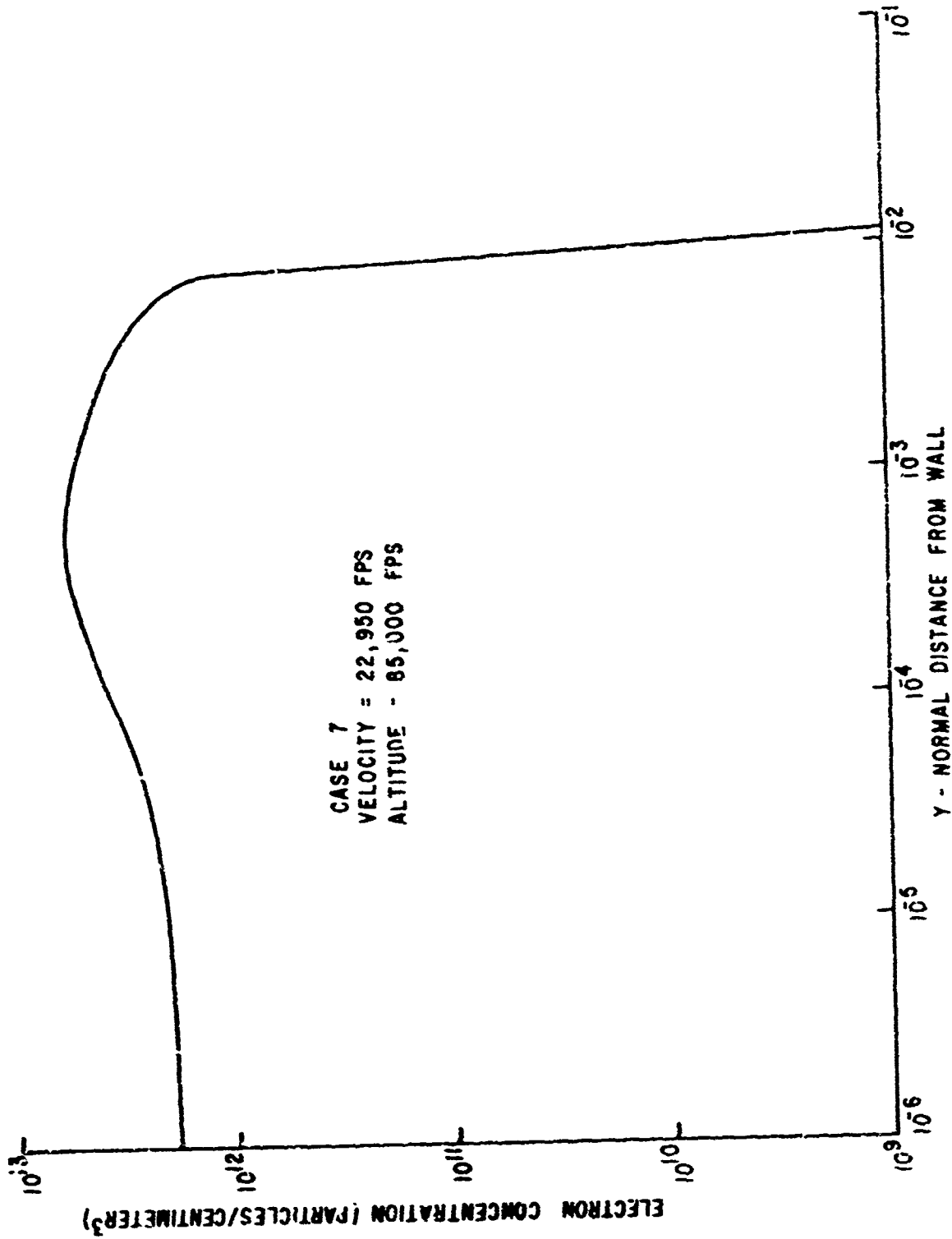


FIGURE 29. NONSIMILAR REENTRY ANALYSIS--BOUNDARY LAYER ELECTRON CONCENTRATION PROFILE.

multicomponent frequency much greater than the constant cross-section frequency in the vicinity of the wall. In the region from  $5 \times 10^{-4}$  feet to approximately  $1.2 \times 10^{-2}$  feet, the electron collisions are predominately with  $H_2O$ ,  $CO_2$ , and  $N_2$ . From  $1.2 \times 10^{-2}$  feet to the edge, the clean air  $N_2$  and  $O_2$  collisions are predominant. The multicomponent collision-frequency curve is observed to correspond to the concentration fluctuations and temperature dependent cross sections of these species in the latter two regions. The divergence of the frequency curves near the edge occurs because there the constant cross-section frequency is inversely proportional to temperature and thus increases as the temperature decreases toward the edge. In contrast, the multicomponent frequency decreases because the concentrations of the large molecules decrease toward the edge and the cross sections of the clean air molecules decrease as the temperature decreases toward the edge.

Although the collision frequency models predict drastically different frequencies in the vicinity of the wall, the attenuation calculations for a 2.5 GHz transmitted signal vary only moderately. The multicomponent model predicted an attenuation of 5.82 dB, and the constant cross-section model predicted 6.65 dB. The constant cross-section value is 14.3 percent higher than the multicomponent value. An explanation for the moderate difference in attenuation calculations is given by the collision frequency curves and the electron-density curve. As in previous cases, the region near the wall where the collision frequencies vary drastically is very thin. The electron density in this region is not extremely large so that attenuation in this region is estimated to be small compared to the attenuation in the remainder of the boundary layer. In the region from approximately  $10^{-2}$  feet to the edge, the electron density is very small and the attenuation is again small. Thus most of the signal attenuation occurs in the region between  $5 \times 10^{-4}$  feet and  $10^{-2}$  feet. The collision frequencies in this region are moderately different and thus moderately different signal attenuations are predicted.

### 3. ROCKET SLED; CASE 8

A final case studied is the boundary layer formed about the nose cone of a hypersonic rocket sled. A rocket sled experiment was designed by AFWL to obtain experimental data to help validate the AFWL nonsimilar chemically reacting turbulent boundary layer code SLIMP. The experiment also established the feasibility of using a rocket sled to form a plasma sheath. The sled nose cone is a sphere cone with a 1/2-inch nose radius and a 9-degree half-angle cone. It has a

tungsten nose tip, and the afterbody is covered with Avcoat 3024 (epoxy urethane, C567 H950 O113 N35) which is a low-performance heatshield material. This material is seeded with 20 percent by weight of  $\text{CsNO}_3$ , which adds easily ionized cesium atoms to the boundary layer.

Results for this nonsimilar boundary layer analysis for a streamwise station of 1.696 feet are shown in figures 30 to 33. Figure 30 shows that the multi-component collision frequency was predicted to be much higher than the constant cross-section collision frequency over a large portion of the boundary layer. As in the previous cases the constant cross-section frequency profile can be directly related to the temperature profile (figure 31). Particle densities (figure 32) in conjunction with cross-section data show that the large  $\text{CO}_2$ ,  $\text{H}_2\text{O}$ , and Cs molecules together with the  $\text{N}_2$  molecule are chiefly responsible for the behavior of the multicomponent collision frequency. Figures 30 and 33 show that the greatest concentration of electrons in the boundary layer occurs in a region where the collision frequencies vary by a factor of approximately two. This large difference is reflected in the signal attenuation calculation. For a two GHz transmitted signal, the multicomponent model predicts an attenuation of 6.80 dB, and the constant cross section model predicts an attenuation of 10.6 dB. The constant cross-section prediction is 56 percent higher than the multicomponent prediction.

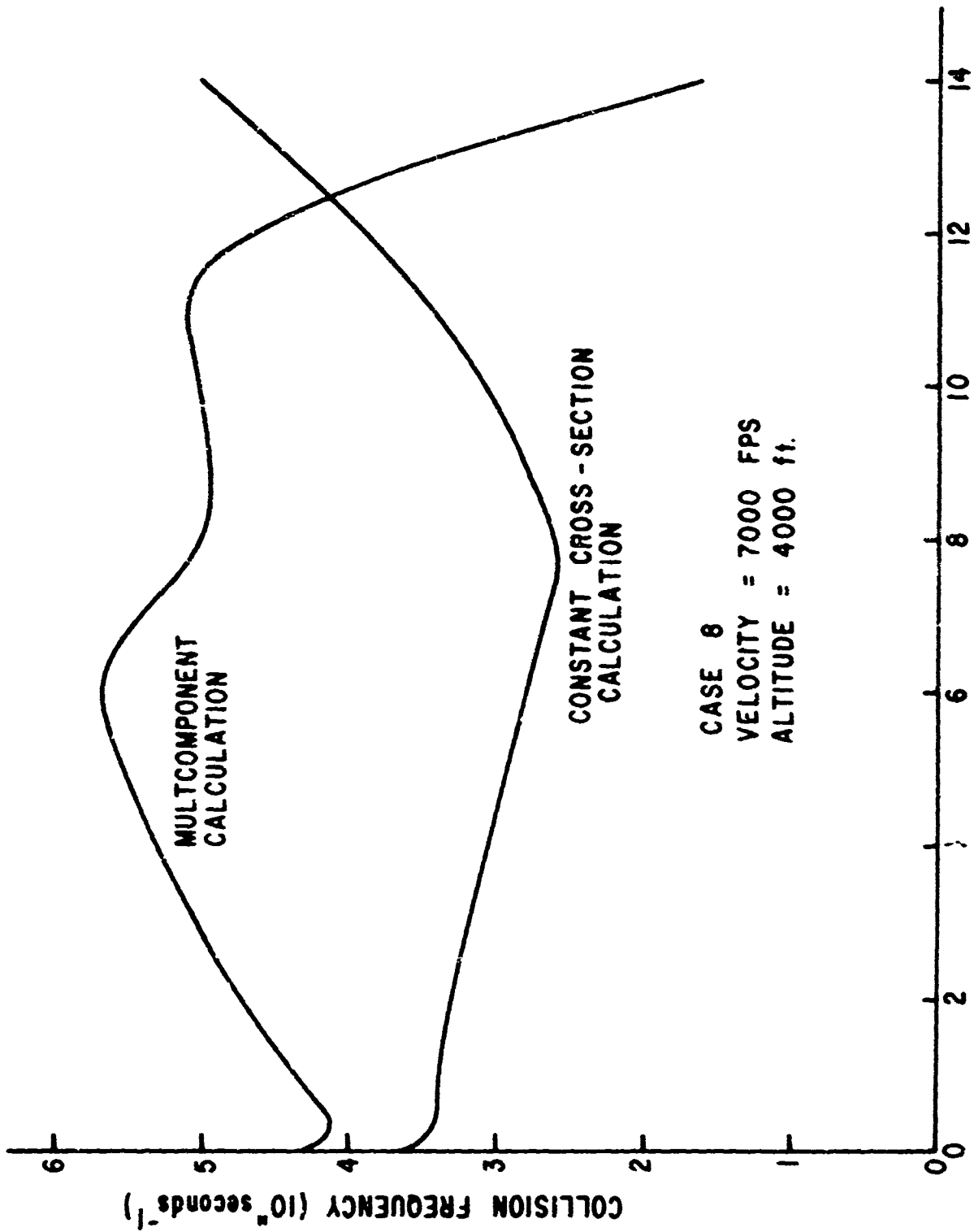


Figure 30. Rocket Sled Analysis--Boundary Layer Collision Frequency Profile

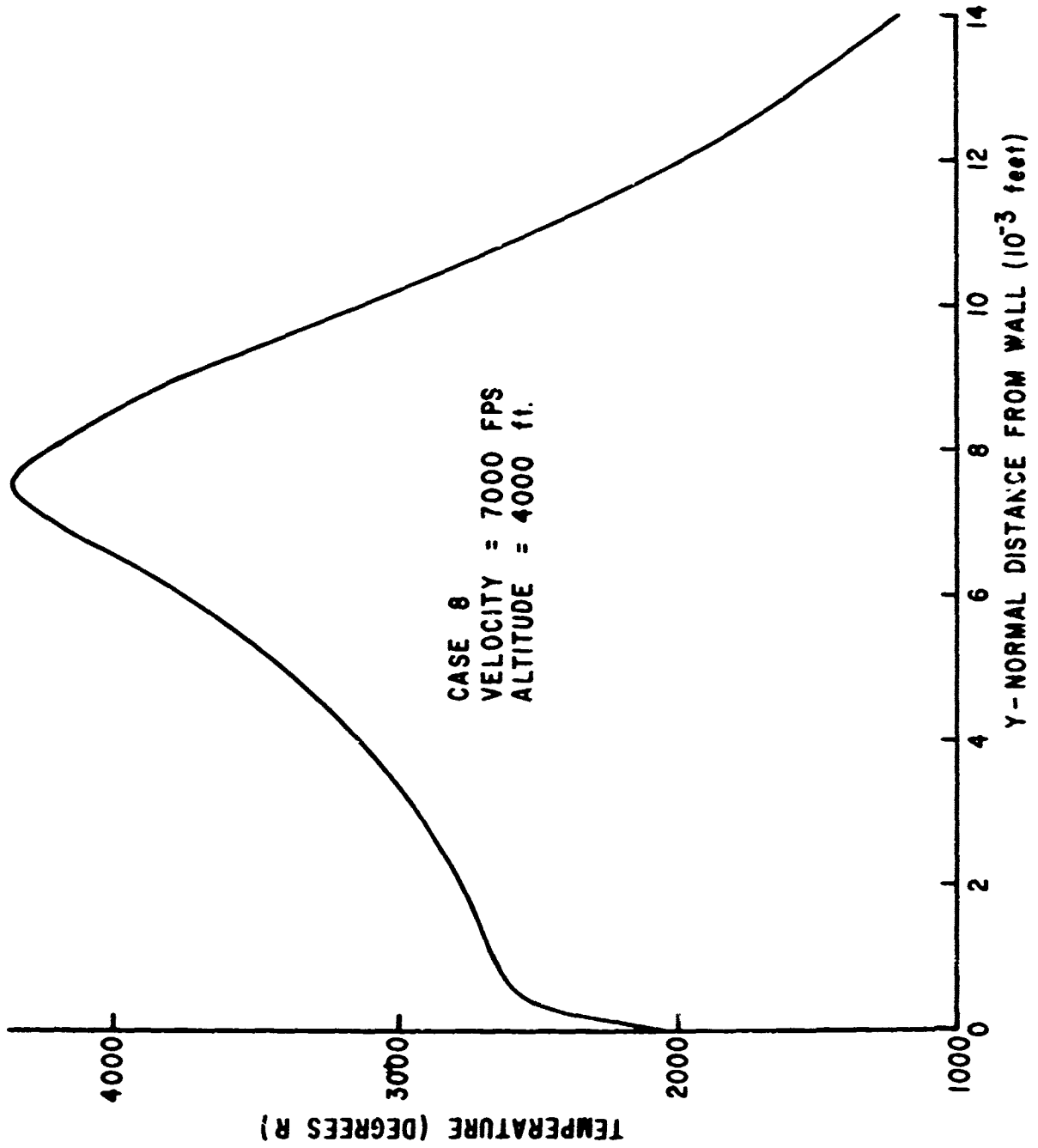


Figure 31. Rocket Sled Analysis--Boundary Layer Temperature Profile

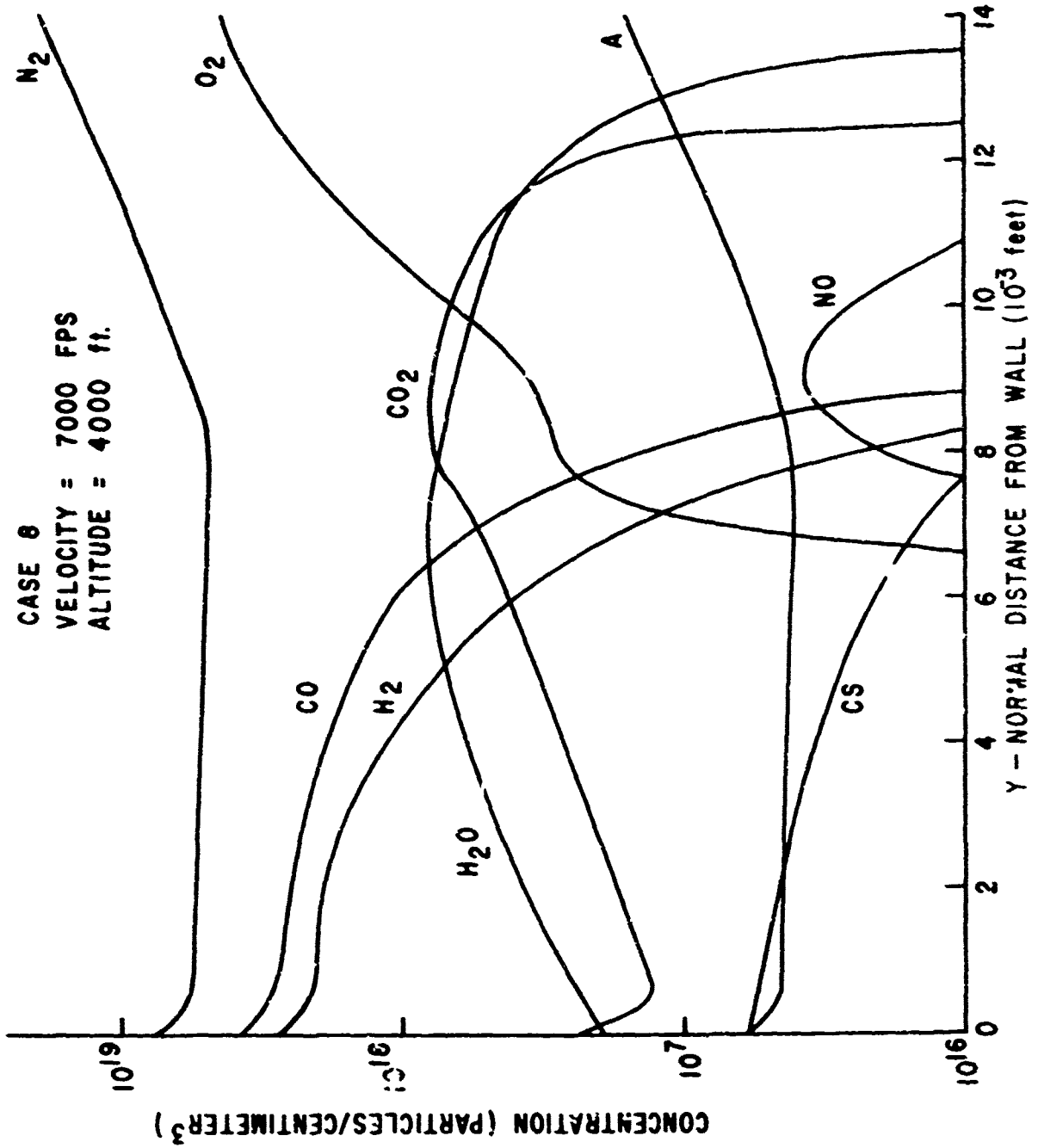


Figure 32. Rocket Sled Analysis--Boundary Layer Species Concentration Profiles

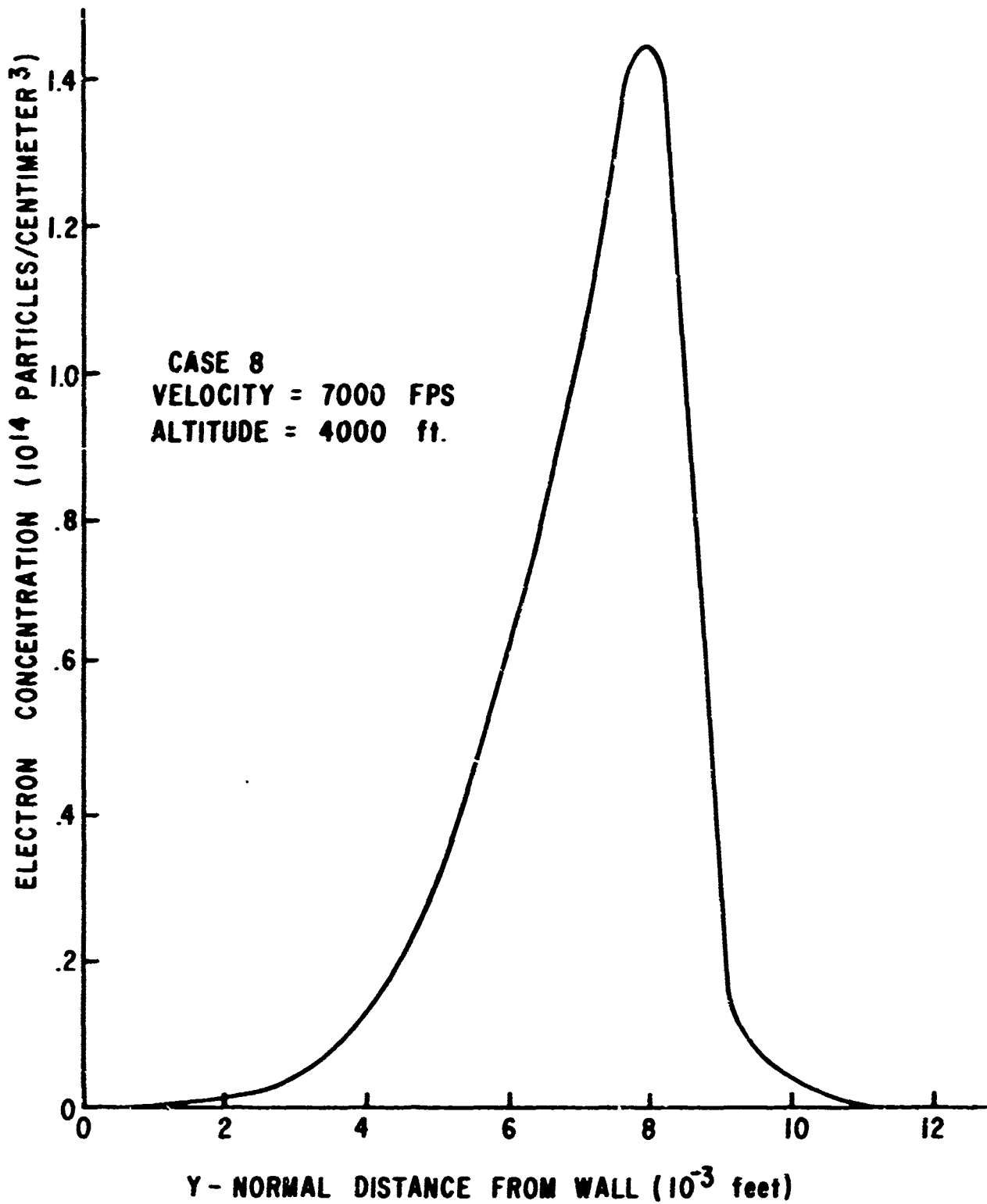


Figure 33. Rocket Sled Analysis--Boundary Layer Electron Concentration Profile

## SECTION V

### CONCLUSIONS AND RECOMMENDATIONS

A parametric study showed that a gaseous mixture of phenolic carbon and air can contain a large variety of chemical species with widely varying collision cross sections. The density and the temperature-dependent cross section of each specie are taken into account by the multicomponent collision frequency model. This model showed that the collision frequency in an ablation air mixture can vary radically as the mass fraction of ablator is varied. Since the constant cross-section model defines collision frequency as a function of only pressure and temperature, the chemical composition of an ablation air mixture has no effect on collision frequency predictions made using this model. The parametric study showed that collision frequency predictions made by the two models can vary significantly. The validity of representing the collision cross sections in an ablation mixture by a single constant cross section is questionable in view of the radical variations of species and thus cross sections with variations of ablator mass fraction. Because the multicomponent model is physically more realistic, it appears to be more reliable than the constant cross-section model for analyzing such mixtures.

Significantly different collision frequencies in a plasma can be predicted by the two models. Near the vehicle wall, large ablation molecules can make the multicomponent collision frequency much larger than the constant cross-section collision frequency. The region of the boundary layer in which the ablation species are important is dependent on ablation rate, molecular species present, and the thermodynamic state. Near the boundary layer edge the ablation species concentrations are low enough to be negligible. Here the constant cross section and multicomponent models can predict significantly different collision frequencies. The cross sections of the clean air species decrease with decreasing temperature. Since the constant cross-section model predicts that collision frequency is inversely proportional to the square root of temperature, the collision frequencies predicted by the two models can diverge in a region, such as toward the boundary-layer edge, where temperature decreases.

Predictions of the transmitted signal attenuation using the two models can vary significantly. For the six trajectory cases examined, the multicomponent

model predicted higher attenuations than the constant cross-section model. The constant cross-section model predicted a collision frequency that was 14.3 percent higher than the multicomponent model for the 85,000 feet altitude coupled chemistry case. The rocket sled case showed the largest difference in attenuation predictions. Because the  $H_2O$ ,  $CO_2$ , and Cs molecules caused large collision frequency deviations in a large region of the boundary layer and because most of the free electrons were concentrated in this region, a large deviation in attenuation predictions occurred. The constant cross-section model predicted an attenuation that was 56 percent higher than the multicomponent attenuation. These cases have shown that the multicomponent attenuation can be significantly higher or lower than the constant cross-section attenuation. These cases have also shown that the variations in attenuation predictions can be less severe than the variations in collision frequency predictions depending on the plasma electron density profile.

The six trajectory cases have shown that significant concentrations of the large ablation molecules may be restricted to an extremely small region of a boundary layer. In cases similar to these, multicomponent collision frequency predictions based on clean air cross sections only may be sufficient to predict signal attenuation. At temperatures from approximately 8000°R to 10,000°R the constant cross section which is used for the constant cross-section model appears to represent the average cross section of clean air with reasonable accuracy. Use of the constant cross-section model to predict collision frequencies at these temperatures should not cause significant error. It may be expected that the contribution of large ablation molecules to the total electron collision frequency will increase with increasing ablation rate. Since the alkali metal contaminants in a heatshield material are the main contributors of free electrons in a boundary layer plasma, the electron density may be expected to increase with increasing ablation rate. It may thus be conjectured that as a signal attenuation increases because of increasing electron density, the contribution of ablation species to the total collision frequency will be increasingly important, and thus, it becomes increasingly important to use the multicomponent model to obtain accurate predictions. An inspection of the product  $n_j Q_{ej}$  for species in a boundary layer can be used to estimate how much detail to include in a collision frequency analysis.

Use of the multicomponent collision frequency model is restricted by two major factors: 1) collision cross sections must be available for important chemical species, and 2) an accurate chemical composition analysis is required.

Only a phenolic carbon ablator has been investigated in this study. Of equal importance are mixtures of phenolic silica and air. Neither analytical or experimental values have been found in the open literature for many of the ablation species that contain silica. It is suspected that collision cross-section data do not exist for many of these molecules. Therefore, fundamental analyses or experimentation to obtain cross-section data should be performed if this model is to be applied to silica materials. The multicomponent model is dependent on species concentrations of a gaseous mixture. It has been shown that small amounts of large molecules can greatly affect the collision frequency. Thus, an accurate analysis of the chemical composition of a gaseous mixture must be obtained before this model can predict a reliable and accurate collision frequency.

## REFERENCES

1. Fivel, H. J., Schaffer, M. J., Young, J. D., User's Manual Turbulent Boundary Layer Program, AFWL-TR-67-141, Vol. V, Air Force Weapons Laboratory, Kirtland AFB, New Mexico, May 1969.
2. Schmidt, H., Thyson, N., Turbulent Boundary Layer Calculations for Ablating Carbon Phenolic Heat Shields, SAMS0-TR-69-85, Avco Corporation, Willington, Massachusetts, June 1969.
3. Anderson, L. W., Kendall, R. M., A Nonsimilar Solution for Multicomponent Reacting Laminar and Turbulent Boundary Layer Flows Including Transverse Curvature, AFWL-TR-69-106, Air Force Weapons Laboratory, Kirtland AFB, New Mexico, March 1970.
4. Hurwitz, T. A., and Whitlow, W. L., User's Manual Transmission Characteristics Program (S036), AFWL-TR-67-141, Vol. VI, Air Force Weapons Laboratory, Kirtland AFB, New Mexico, to be published.
5. Chapman, S., Cowling, T. G., The Mathematical Theory of Non-Uniform Gases, Cambridge University Press, New York, 1970.
6. Brown, S. C., Basic Data of Plasma Physics, The M.I.T. Press, Cambridge, Massachusetts, 1966.
7. Hasted, J. B., Physics of Atomic Collisions, Butterworths, Washington, DC, 1964.
8. Shkanofsky, I. P., Bachynski, M. P., Johnston, T. W., Collision Frequency Associated with High-Temperature Air and Scattering Cross Sections of the Constituents, RCA Victor Company Research Report No. 7-801,5, December 1959.
9. Massey, H. S. W., Burhop, E. H. S., Gilbody, H. B., Electronic and Ionic Impact Phenomena, Vol. I and II, Oxford Press, London, 1969.
10. Kieffer, L. J., Bibliography of Low-Energy Electron Collision Cross-Section Data, Boulder, Colorado, March 1967.
11. Chamberlain, G. E., Kieffer, L. J., Bibliography of Low-Energy Electron Collision, Joint Institute for Laboratory Astrophysics (JILA) Information Center Report No. 10, National Bureau of Standards, Boulder, Colorado, February 1970.
12. Phelps, A. V., Electron Collision Frequencies and Radio Frequency Absorption in Air, DASA 1948, Westinghouse Research Laboratories, September 1968.
13. Musal, H. H., Electron Collision Frequency in Equilibrium High-Temperature Air, U. S. Army Rocket and Guided Missile Agency, Plasma Physics Study, Research Note 9, Bendix Aviation Corporation, May 1960.

## REFERENCES (cont'd)

14. Engelhardt, A. G., Phelps, A. V., Risk, C. G., "Determination of Momentum Transfer and Inelastic Collision Cross Sections for Electrons in Nitrogen Using Transport Coefficients," Physical Review, Vol. 28, No. 7, pp. A1566-A1574. July 1957.
15. Lamb, L., Lin, S. C., "Electrical Conductivity of Thermally Ionized Air Produced in a Shock Tube," Journal of Applied Physics, Vol. 28, No. 7, pp. 754-759, July 1957.
16. Klein, M. M., Bruekner, K. A., "Interaction of Slow Electrons with Atomic Oxygen and Atomic Nitrogen," Physical Review, Vol. 3, pp. 1115-1120, August 1958.
17. Hammerling, P., Shine, W. W., Kivel, B., "Low-Energy Elastic Scattering of Electrons by Oxygen and Nitrogen," Journal of Applied Physics, Vol. 28, No. 7, pp. 760-764, July 1957.
18. Bayes, K. D., Kivelson, D., Wong, S. C., "Measurements of Cyclotron Resonance of Molecular Cross Sections for Elastic Collisions with 295°K Electrons," Journal of Chemical Physics, Vol. 37, pp. 1217-1225, September 1962.
19. Hake, R. D., Phelps, A. V., "Momentum-Transfer and Inelastic Collision Cross Sections for Electrons in O<sub>2</sub>, CO, CO<sub>2</sub>," Physical Review, Vol. 158, No. 1, pp. 70-84, June 1967.
20. Pack, J. L., Vohall, R. E., Phelps, A. V., "Drift Velocities in Slow Electrons in Krypton, Xenon, Deuterium, Carbon Monoxide, Carbon Dioxide, Water Vapor, Nitrous Oxide, and Ammonia," Physical Review, Vol. 127, No. 6, pp. 2084-2088, September 1962.
21. Takeda, S., Dougal, A. A., "Microwave Study of Afterglow Discharge in Water Vapor," Journal of Applied Physics, Vol. 31, No. 2, pp. 412-416, February 1960.
22. Engelhardt, A. G., Phelps, A. V., "Elastic Photodetachment from Ions and Elastic Collision Cross Sections for O, C, Cl, and F," Physical Review, Vol. 126, No. 4, pp. 2115-2119, September 1963.
23. Demetriades, S. T., Fonda-Bonardi, G., Argyropoulos, G. S., Experimental Determination of Collision Cross Sections for Momentum Transfer, OSR 69-2809 TR, Air Force Office of Scientific Research, Washington, DC, September 1969.
24. Cooper, J. W., Martin, J. B., "Electron Photodetachment from Ions and Elastic Collision Cross Sections for O, C, Cl and F," Physical Review, Vol. 126, No. 4, pp. 1482-1488, May 1962.